TOPICAL REVIEW — Magnetism, magnetic materials, and interdisciplinary research

# Colossal magnetoresistance in manganites and related prototype devices*

Liu Yu-Kuai(刘愉快), Yin Yue-Wei(殷月伟)†, and Li Xiao-Guang(李晓光)‡

*Hefei National Laboratory for Physical Sciences at Microscale, Department of Physics, University of Science and Technology of China, Hefei* 230026, *China*

(Received 5 June 2013)

We review colossal magnetoresistance in single phase manganites, as related to the field sensitive spin–charge interactions and phase separation; the rectifying property and negative/positive magnetoresistance in manganite/Nb:$SrTiO_3$ p–n junctions in relation to the special interface electronic structure; magnetoelectric coupling in manganite/ferroelectric structures that takes advantage of strain, carrier density, and magnetic field sensitivity; tunneling magnetoresistance in tunnel junctions with dielectric, ferroelectric, and organic semiconductor spacers using the fully spin polarized nature of manganites; and the effect of particle size on magnetic properties in manganite nanoparticles.

**Keywords:** colossal magnetoresistance manganite, multiferroic heterostructure, tunnel junction, size effect

**PACS:** 75.47.Gk, 75.85.+t, 73.43.Jn, 75.75.–c **DOI:** 10.1088/1674-1056/22/8/087502

## 1. Introduction

The perovskite manganite $RE_{1-x}AE_xMnO_3$ ($RE$ = La, Pr, Sm, etc. and $AE$ = Ca, Sr, Ba, Pb) exhibiting colossal magnetoresistance (CMR) is a strongly correlated electron system with strong interactions among the charge, spin, orbital, and lattice degrees of freedom, such as double-exchange interaction, super-exchange interaction, Jahn–Taller-type electron–lattice distortion, Hund's coupling, etc., leading to complex electronic, magnetic, and structural phase diagrams. The rich physics involved in manganites, for example, the phase separation, charge ordering, and half-metallicity, makes it one of the hottest topics in condensed matter physics, and various prototype devices have been designed, following upon the development of the preparation technology and scientific research.

The discovery of colossal magnetoresistance (CMR) in divalent alkaline-earth ion-doped perovskite manganites $RE_{1-x}AE_xMnO_3$, where $RE$ is a trivalent rare-earth (La, Pr, Sm, etc.) and $AE$ is a divalent alkaline-earth ion (Ca, Sr, Ba), has aroused tremendous interest due to their rich fundamental physics and great potential application in spintronics.[1–9] In fact, the magnetoresistance (MR) effect (the magnitude of which is typically defined as

$$\mathrm{MR}(H) = \frac{|\rho(H) - \rho(0)|}{\rho(H)},$$

where $\rho(H)$ and $\rho(0)$ represent the resistivities with and without magnetic field) in perovskite manganites was already known early in the 1960s. For example, in 1969, a thorough MR investigation as well as a phenomenological analysis was reported for $La_{1-x}Pb_xMnO_3$ crystals.[10] However, only since mid-1990s has an enormous amount of work[5,8] been devoted to the manganites, after the discovery of so-called CMR in manganites (e.g., up to $1.27 \times 10^5$% in $La_{2/3}Ca_{1/3}MnO_3$ thin film at 77 K and 6 T).[11] Now, it is generally believed that the underlying origin of CMR is closely related to the nature of CMR manganites which are strongly correlated electron systems with interplay among the lattice, spin, charge, and orbital degrees of freedom, such as double exchange interaction, Jahn–Taller effect, electronic phase separation, and charge ordering. The work has been extensively described in some review papers.[1–9]

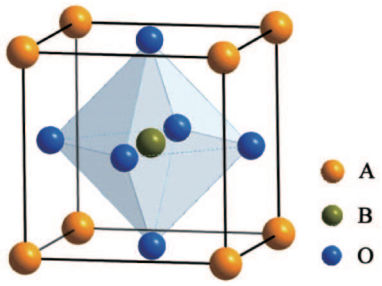



**Fig. 1.** Schematic structure of the cubic perovskite $ABO_3$.

The structure of $RE_{1-x}AE_xMnO_3$ manganite is close to cubic perovskite ($ABO_3$), as schematically shown in Fig. 1. The $RE$ trivalent and $AE$ divalent ions occupy the A-site with 12-fold oxygen coordination, while the smaller Mn ion at the B site is located at the center of an oxygen octahedron with 6-fold coordination. Generally, the perovskite-based

*Project supported by the National Natural Science Foundation of China and the National Basic Research Program of China (Grant Nos. 2012CB922003, 2011CBA00102, and 2009CB929502).

†Corresponding author. E-mail: yyw@ustc.edu.cn

‡Corresponding author. E-mail: lixg@ustc.edu.cn

© 2013 Chinese Physical Society and IOP Publishing Ltd 

$RE_{1-x}AE_x$MnO$_3$ material shows lattice distortions as modifications from the cubic structure. A possible lattice deformation comes from the connective pattern of the MnO$_6$ octahedral in the perovskite structure, which is revealed by the so-called tolerance factor $t = (r_B + r_O)/\sqrt{2}(r_A + r_O)$, where $r_i$ ($i$ = A, B, and O) represents the ionic size of each element.[12]

Another lattice distortion is the deformation of the MnO$_6$ octahedral arising from the Jahn–Teller (JT) effect, which changes the electronic structure of manganite, as shown in Fig. 2.[13] Due to the crystal field, five degenerate 3d orbitals on the Mn-sites are subject to a partial lifting of the degeneracy into three lower-lying $t_{2g}$ orbitals and two higher-lying $e_g$ orbitals. When the occupied electrons at both orbitals are smaller than the degeneracy of the $t_{2g}$ and $e_g$ levels, the $t_{2g}$ and $e_g$ orbitals will be lifted as shown in Fig. 2, i.e., the JT effect. In $RE_{1-x}AE_x$MnO$_3$ manganite, the valance states of Mn ions are of the mixture with $Mn^{3+}$ (with three $t_{2g}$ and one $e_g$ electrons) and $Mn^{4+}$ (with three $t_{2g}$ electrons only), and the proportions of Mn ions for the valence states 3+ and 4+ are $x$ and $1-x$, respectively.

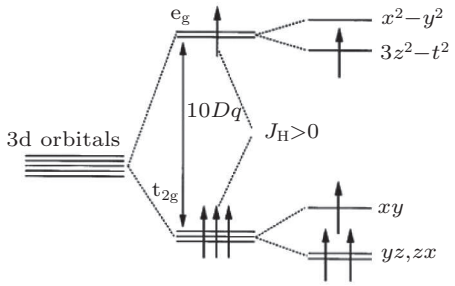



**Fig. 2.** Schematic illustration of the electronic structure of $Mn^{3+}$ ions in MnO$_6$ octahedron with Jahn–Teller effect.[13]

The transfer of $e_g$ electron from $Mn^{3+}$ to $Mn^{4+}$ is the basic mechanism of electrical conduction in manganites, governed by double exchange (DE) interaction (the simultaneous jumps of the $e_g$ electron of $Mn^{3+}$ to the O p-orbital and the electron with same spin from the O p-orbital to the empty $e_g$ orbital of $Mn^{4+}$) leading to an FM state.[14] In manganites with strong DE interaction (e.g. $La_{1-x}Sr_xMnO_3$ with $x = 1/3$), the $e_g$ electrons become delocalized for a certain doping range at low temperature, leading to a metallic behavior.[15] Because the DE interaction can be enhanced in a magnetic field by aligning the spins at adjacent Mn–O–Mn ions, the conductivity will increase, resulting in negative magnetoresistance. The FM in combination with Hund's coupling, which removes the spin degeneracy in the FM state, allows the separation of the spin-up ($e_g^{\uparrow}$, $t_{2g}^{\uparrow}$) and spin-down ($e_g^{\downarrow}$, $t_{2g}^{\downarrow}$) bands as schematically shown in Fig. 3.[16] One can see that the electrons almost occupy the $e_g^{1\uparrow}$ band near the Fermi level, leading to half-metallic behavior. This fully spin-polarized condition has great potential for spin electronics.[17] It is also notable that the strength of Hund's coupling can change the electronic structure, resulting a higher $t_{2g}^{\downarrow}/e_g^{2\uparrow}$ band with strong/weak Hund's coupling, as shown in Figs. 3(a) and 3(b).

Besides the DE interaction and Hund's coupling, there are also some other important factors affecting the physical properties of manganites, such as the electron–lattice interaction, FM/antiferromagnetic (AFM) super-exchange (SE) interaction between the local spins, inter-site exchange interaction between the $e_g$ orbitals (orbital ordering tendency), and intra-site and inter-site Coulomb repulsion interaction between the $e_g$ electrons, etc.[9] These interactions/instabilities compete with the ferromagnetic DE interaction, producing complex electronic phases.

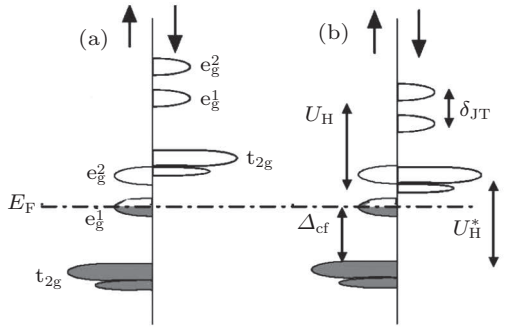



**Fig. 3.** Schematic diagram of spin-dependent (large arrows) density of states. (a) Strong Hund's coupling ($U_H^* > \Delta_{cf} + \delta_{JT}$), and (b) weak Hund's coupling ($U_H^* < \Delta_{cf} + \delta_{JT}$). Here, $\Delta_{cf}$ and $\delta_{JT}$ represent the energies of the crystal field splitting and JT distortion splitting, respectively. $U_H$ or $U_H^*$ denotes the separation between $e_g^{\uparrow}$ and $t_{2g}^{\uparrow}$ or $e_g^{\downarrow}$ and $t_{2g}^{\downarrow}$ bands, and $E_F$ represents the Fermi level.[16]

Taking $La_{1-x}Ca_xMnO_3$ as an example, the representative electronic phase diagram is shown in Fig. 4.[7] For $La_{1-x}Ca_xMnO_3$ ($0 < x < 0.1$) with a small amount of $Mn^{4+}$, the DE interaction is weak and the Coulomb expulsion among $Mn^{3+}$ hinders the hopping of $e_g$ electrons, leading to the material's insulating nature; while the super-exchange coupling (usually antiferromagnetic coupling between two next-nearest-neighbor Mn cations through the non-magnetic O anion) between $Mn^{3+}$ ions causes canted antiferromagnetic (CAF).[18] For $0.1 < x < 0.2$, the competition between the DE interaction and super-exchange interaction results in an insulating ferromagnetism below a certain temperature, and at a still lower temperature, the charge ordered (CO) state appears.[19] The CO state with ordered $Mn^{3+}$ and $Mn^{4+}$ in real space is probably due to long-range Coulomb interaction,[20] JT phonons interaction,[21] or super-exchange interaction,[22] but the intrinsic mechanism is still controversial.[9] With a further increase of the dopant concentration $x$, the ferromagnetic metal state appears below the ferromagnetic Curie temperature ($T_C$) with a maximum $T_C$ at $x = 3/8$.[23] In this region, the system undergoes an insulator–metal transition as the temperature crosses $T_C$ which moves to higher temperatures in magnetic field ($H$). For $x > 0.5$, the CO transition

($T_{CO}$) is observed at temperatures higher than the $T_{CO}$ for $0.1 < x < 0.2$, and is accompanied by an antiferromagnetic state in the low-temperature range.[24,25] When $x > 7/8$, the CO state in $La_{1-x}Ca_xMnO_3$ disappears, and the low temperature state becomes CAF again.

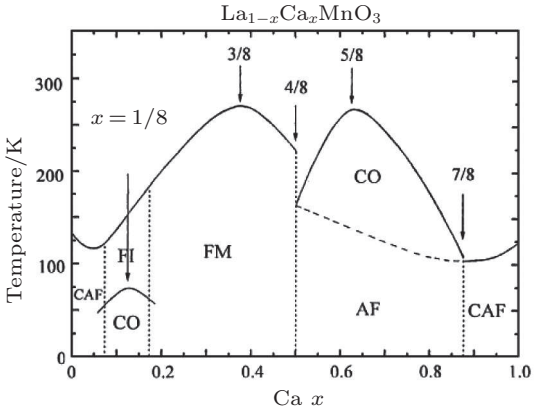



**Fig. 4.** Magnetic and electronic phase diagrams of $La_{1-x}Ca_xMnO_3$. The various states are: ferromagnetic insulating (FI), ferromagnetic (FM), canted antiferromagnetic (CAF), and charge-ordered (CO).[7]

It is worth mentioning that the phase boundaries are not strictly clear as these phases always coexist and compete with each other, which has been experimentally observed by different characterization methods, e.g., the coexistence of paramagnetic (PM) insulating and FM metallic phases in $La_{0.7}Ca_{0.3}MnO_3$, detected by scanning tunneling spectroscopy,[26] the FM metallic and CO insulating phases in $La_{5/8-y}Pr_yCa_{3/8}MnO_3$ ($0 < y < 0.4$) by electron microscopy,[27] the FM metallic and FM insulating phases in $La_{1-x}Ca_xMnO_3$ with $0.2 < x < 0.5$ by $^{55}Mn$ nuclear magnetic resonance (NMR),[28] and the antiferromagnetic CO structure and FM in $La_{0.35}Ca_{0.65}MnO_3$ by NMR.[29] Thus, theoretical and experimental researches are rapidly converging to a unified picture of the physics of manganites in the CMR regimes being clearly dominated by inhomogeneities in the form of coexisting competing phases.[9]

Therefore, because doped manganites exhibit a rich phase diagram as a function of doped concentration $x$ and the phase separation is sensitive to magnetic fields, the manganites can be used to construct magnetoelectric coupling devices to serve as high sensitivity magnetic sensors.[30,31] In addition, the occurrence of metallic phases with a fully spin polarized conduction band is another important feature manganites showing their promise for applications in spintronics.[17] Many prototype devices have been designed by using the half-metallic property of manganites, such as magnetic tunnel junctions[32] and spin detectors in spin valve devices.[33]

In the present article, after a discussion on the CMR effect in single phase manganites, special attention is devoted to the new prototype devices based on CMR materials with heterostructure, including p–n junctions, magnetoelectric coupling devices, magnetic tunnel junctions, multiferroic tunnel junctions, spin-detectors in spin-valves. Then, the size effect in nanosized manganites is introduced. Since the research area is broad and rapidly developing, an extensive amount of research on various manganites has been published every year, so we apologize in advance to the authors of those that have unfortunately not been cited here.

## 2. Single phase

### 2.1. Colossal magnetoresistance and phase-separation model

Figure 5 shows the magnetic field dependence of the resistivity for $La_{0.67}Ca_{0.33}MnO_x$ epitaxial thin films at different temperatures.[34] One can see that the films exhibit a negative ($\rho(H) < \rho(0)$) CMR effect up to $1.27 \times 10^5\%$ at 77 K and 6 T. After being annealed at 850 °C/1 h in a 3-atm (1 atm = $1.01325 \times 10^5$ Pa) oxygen atmosphere, Jin *et al.* found that the CMR ratio of $La_{0.67}Ca_{0.33}MnO_x$ thin film can be increased from $3.9 \times 10^4\%$ to $1.1 \times 10^6\%$ at 110 K and 6 T.[35] The CMR effect is closely related to the field-sensitive complex electron–electron and electron–lattice effects in manganites, which will result in tremendous conductivity variation in magnetic fields. In addition, the insulating/metallic phase separation is another field-dependent factor critical for the observed CMR effects. Both experimental and theoretical studies have shown that the typical length scale for phase-separation in manganites is from several nanometers to submicrometer scale, depending on the material and the dopant level.[27,36–40]

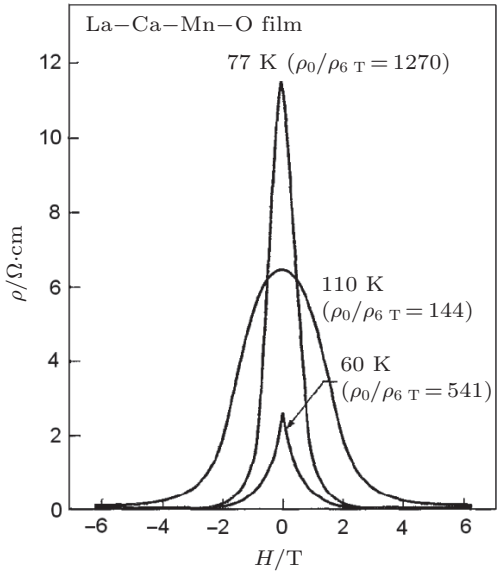



**Fig. 5.** Magnetic field dependence of resistivity of $La_{0.67}Ca_{0.33}MnO_3$ thin film at different temperatures.[34]

Figure 6 shows the local conductivity of the $La_{0.7}Ca_{0.3}MnO_3$ single films just below $T_C$, observed by scanning tunneling spectroscopy at different magnetic fields.[26] The light colors correspond to the insulating region, whereas

the dark colors represent metallic characteristics. By applying a magnetic field, a considerable fraction of the insulating regions can be converted into metallic percolation paths and the resistance will be suppressed accordingly, leading to a significant negative magnetoresistance effect. This evolves faster in low magnetic fields ($\leq 1$ T) and continues to develop up to 9 T. In addition, with decreasing temperature, the system becomes more metallic on average. This phase separation in a wide temperature range is observed in $La_{0.7}Ca_{0.3}MnO_3$ single films, in which the metallic and insulating areas are strongly dependent on both temperature and magnetic field.[26] Similar phase separation phenomena were found in $Pr_{0.5}Sr_{0.5}MnO_3$,[41] $Pr_{1-x}Ca_xMnO_3$,[42] $Nd_{1-x}Sr_xMnO_3$,[43] $La_{0.45}Sr_{0.55}MnO_{3-\delta}$,[44,45] etc.

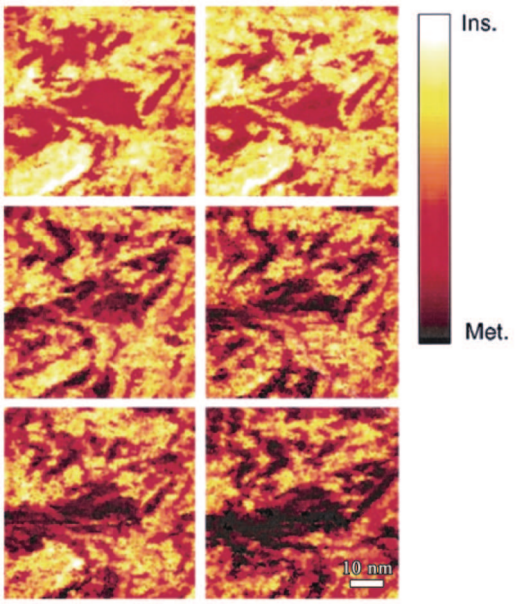



**Fig. 6.** Generic spectroscopic images of the local electronic structure of $La_{0.7}Ca_{0.3}MnO_3$ single films taken just below $T_C$ in magnetic fields of 0, 0.3, 1, 3, 5, and 9 T (from left to right and top to bottom). Parts of the surface are insulating (light colors), whereas others are metallic (dark colors) or in an intermediate state.[26]

A phenomenological model was proposed to describe the relationship between the phase separation and CMR in manganites.[46,47] For example, in an FM metallic/PM insulating phase-separated system, the total resistance can be considered as a serial combination of the resistance of the coexisting phases and written as[46]

$$R = f_{\rm FM}R_{\rm FM} + (1 - f_{\rm FM})R_{\rm PI}, \quad (1)$$

where $f_{\rm FM}$ and $(1 - f_{\rm FM})$ are the volume fractions, and $R_{\rm FM}$ and $R_{\rm PI}$ are the resistances of the FM metallic and PM insulating phases, respectively. The temperature dependence of $f_{\rm FM}$ obeys a two-energy-level Boltzmann distribution as:

$$f_{\rm FM} = 1/[1 + \exp(\Delta U/k_{\rm B}T)], \quad (2)$$

$$\Delta U = -U_0(1 - T/T_{\rm C}^{\rm mod}), \quad (3)$$

where $\Delta U$ is the energy difference between the FM metallic and PM insulating phases, $U_0$ is the energy difference between the FM metallic and PM insulating phases at $T = 0$ K, and $T_{\rm C}^{\rm mod}$ (close to $T_{\rm C}$) is the fitted insulator-to-metal transition temperature used in the phenomenological model. The metallic resistance $R_{\rm FM}$ is related to the residual resistance $R_0$, single-magnon's scattering $AT^2$ and electron–phonon interaction $BT^5$, respectively. Specifically, $R_{\rm FM} = R_0 + AT^2 + BT^5$,[48,49] while the resistance $R_{\rm PI}$ can be described as $R_{\rm PI} = C\exp(E_{\rm g}/k_{\rm B}T)$ in terms of the magnetic polaron picture, where constants $A$, $B$, and activation energy $E_{\rm g}$ are magnetic field-dependent and become smaller due to the suppression of single-magnon scattering in FM metallic regions and the formation of magnetic polarons in PM insulating regions under a magnetic field.[50] Thus, resistivity decreases and CMR appears.

Liu *et al.* have employed this model to analyze the magnetic transport data of $La_{5/8}Ca_{3/8}MnO_3$ film.[51] Figure 7(a) shows that the metal–insulator transition temperature is about $T_C = 220$ K at zero magnetic field and increases significantly with increasing magnetic field. The temperature and magnetic field dependencies of resistance in $La_{5/8}Ca_{3/8}MnO_3$ can be well fitted (solid lines) by using Eqs. (1)–(3) based on the above model, as shown in Fig. 7(a). The temperature dependence of the ferromagnetic volume fraction $f_{\rm FM}$ in different magnetic fields is shown in Figs. 7(b) and 7(c), where the volume fraction $f_{\rm FM}$ of the FM metallic phase is significantly enhanced near $T_C$ with increasing magnetic field. It is clear that $f_{\rm FM}$ is close to 1 or zero at temperatures well below or above $T_{\rm C}^{\rm mod}$, and increases with increasing magnetic field, especially around $T_{\rm C}^{\rm mod}$. As a result, the CMR effect manifestly appears.

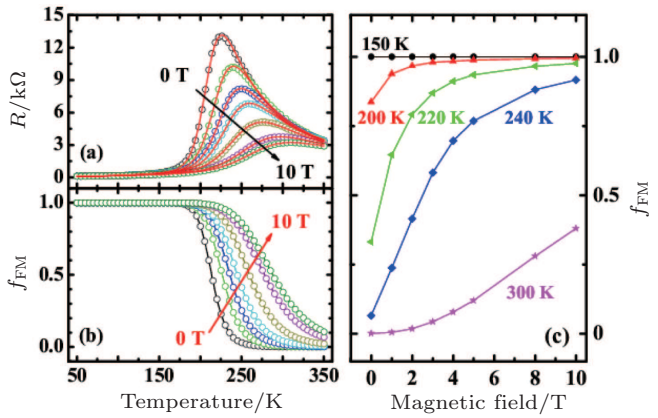



**Fig. 7.** (a) Temperature dependencies of (a) resistance and (b) volume fraction of FM for $La_{5/8}Ca_{3/8}MnO_3$ film in 0, 1, 2, 3, 5, 8, and 10 T. The solid red lines in panel (a) are the fitting results using Eqs. (1)–(3). (c) Magnetic field dependencies of $f_{\rm FM}$ at different temperatures.[51]

The magnetic field dependencies of $T_{\rm C}^{\rm mod}$, $E_{\rm g}$, and $U_0$ are shown in Fig. 8. $T_{\rm C}^{\rm mod}$ increases with increasing magnetic fields as expected, see Fig. 8(a). The monotonous decrease of $E_{\rm g}$ in Fig. 8(b) is due to the fact that the ability of the magnetic polarons to trap electrons is weakened as the spins in the

polarons attempt to align along the magnetic field, which will suppress spin-disorder scattering. The field-dependent $E_g$ can be fitted (solid line of Fig. 8(b)) by

$$E_g(H)/k_B = E_g(0)/k_B - \alpha H^2, \quad (4)$$

where $E_g(0)/k_B = 1002$ K and $\alpha = 2.6$ K/T$^2$ are the fitting parameters. As for the $U_0(H)$, its variation with magnetic fields follows the equation

$$U_0(H)/k_B = \beta \exp(-H/H_0) + U_0(0)/k_B, \quad (5)$$

here, $\beta$, $H_0$, and $U(0)/k_B$ are constant, as shown in Fig. 8(c). With increasing magnetic field, the increase of $f_{FM}$ and decrease of both $E_g$ and $U_0$ confirm that the external magnetic field makes the PM insulating regions change to FM metallic regions. It implies that the competition between the FM metallic and PM insulating phases plays an important role in the CMR effect. It is worth mentioning that, instead of a smooth metallic-insulating phase transition around $T_C$, there is an ultra-sharp peak resistivity at metal–insulator transition temperature in $La_{5/16}Pr_{5/16}Ca_{3/8}MnO_3$ wires with a width comparable to the mesoscopic phase separation domains, resulting from the sudden transition between metallic and insulating states in the domain upon magnetic field and/or temperature change.[52–54]

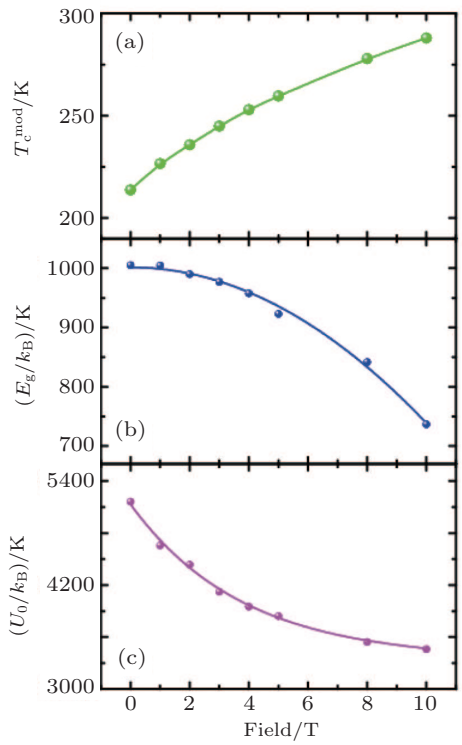



**Fig. 8.** Magnetic field dependencies of $T_C^{mod}$ (a), and $E_g/k_B$ (b), and $U_0/k_B$ (c). The solid lines of panels (b) and (c) are plotted according to Eqs. (4) and (5).[51]

### 2.2. Magnetic field induced melting of charge ordered states

It is well known that the $RE_{1-x}AE_xMnO_3$ manganites (e.g. $La_{1-x}Ca_xMnO_3$ with $0.5 \leq x \leq 0.9$) become insulating below the charge ordered transition temperature $T_{CO}$, because $e_g$ electrons accompanied by their JT distortions freeze in a static order followed by a long-range antiferromagnetic spin order at Néel temperature $T_N \leq T_{CO}$. However, the real-space order of $e_g$ electrons can be destroyed by magnetic field, which will cause an insulator–metal transition below $T_{CO}$ due to the strong spin–charge coupling, thus leading to another kind of CMR effect.[9,55–60]

Figure 9 shows the temperature dependencies of the resistivity $\rho(T)$ at different magnetic fields for $La_{1-x}Ca_xMnO_3$ ($0.5 \leq x \leq 0.9$) series.[61] With decreasing temperature, the zero-field $\rho(T)$ curve for $x = 0.5$ shows a semiconductor-like behavior, but with a discernible change in the slope near $T_{CO}$ signaling the onset of the formation of the CO state, as shown in Fig. 9(a). With magnetic field increasing from 0 T to 6 T, resistivity is reduced slightly, but for 6 T$< H \leq 11$ T resistivity decreases dramatically, although the material still remains semiconductor-like. For $H > 12$ T, a distinct change of $\rho(T)$ induced by magnetic field appears, and a metal–insulator transition occurs around 150 K, which can be viewed as a sign of the collapse of the CO state, resulting in CMR.[62] Similar effects were observed for $x = 0.55$ but the material's insulating behavior persists in 14-T magnetic field (Fig. 9(b)). In contrast with the observations for $x = 0.5$ and 0.55, in samples with $x$ from 0.6 to 0.83, $\rho(T)$ and $T_{CO}$ are almost unchanged for fields up to 14 T, especially for $x = 0.75$, as shown in Figs. 9(c) and 9(d), indicating the robustness of the ordered state near 0.75. With the Ca concentration further increased to $x > 0.83$, $\rho(T)$ becomes weakly field-dependent;[63] see Fig. 9(d).

To quantitatively characterize the doping level dependence of the CMR effect and the stability of the CO state, Qian *et al.* analyzed the MR effect at $H = 14$ T and $T = 75$ K and the change of $\Delta T_{CO}$ ($\Delta T_{CO} = T_{CO}(0\text{ T}) - T_{CO}(14\text{ T})$) for $La_{1-x}Ca_xMnO_3$ ($0.5 \leq x \leq 0.9$), as shown in Figs. 10(a) and 10(b).[63] It can be seen that the MR effect is the largest, on the order of $10^5$ for $x = 0.5$, and drops rapidly as $x$ increases from 0.5 to 0.7. Near $x = 0.75$, the MR effect is minimized and the CO state is most stable. For $x > 0.8$, the weakened CO state becomes sensitive to external magnetic field again, and the MR effect increases with increasing $x$. Further investigations of the magnetic properties, ultrasonic attenuation, and specific heat of charge-ordered $La_{1-x}Ca_xMnO_3$ ($0.55 \leq x \leq 0.87$)[63] reveal that: (i) The peak value $M_P$ obtained from the temperature dependence of the magnetization curve at $T_{CO}$ is a minimum for the $x = 0.75$ sample, as shown in Fig. 10(c), indicating the strength of the ferromagnetic fluctuation is the weakest near $x = 0.75$ which is consistent with the variation of $\rho(T)$ in magnetic fields (Fig. 9(c)). (ii) The JT coupling energy $E_{JT}$ obtained from the ultrasonic attenuation measurements shows a maximum for $x = 0.75$, see Fig. 10(d), consistent with the change of the latent heat $\Delta Q(T_{CO})$ at $T_{CO}$, which

confirms again that the CO state for $x = 0.75$ is the most stable in $La_{1-x}Ca_xMnO_3$ ($0.55 \leq x \leq 0.87$).[63]

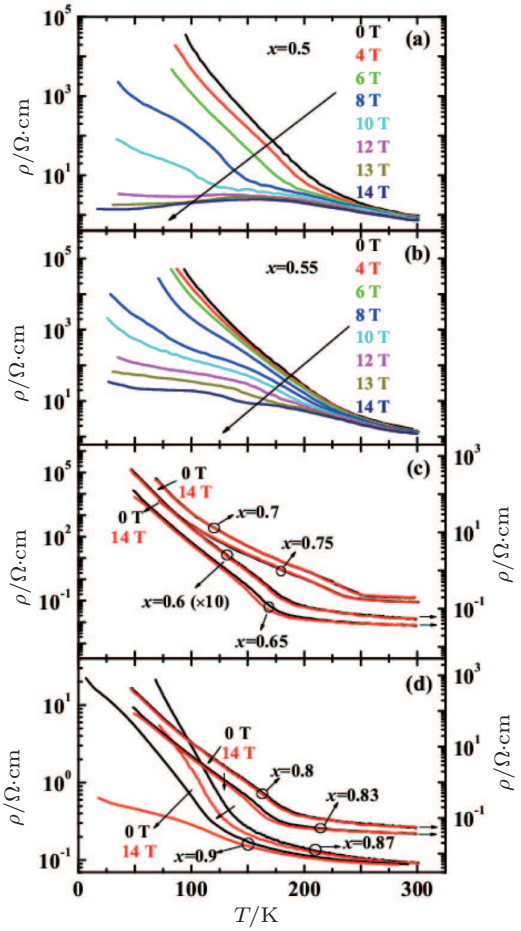



**Fig. 9.** Variations of resistivity with temperatures at different magnetic fields up to 14 T for $La_{1-x}Ca_xMnO_3$ ($x = 0.5$, 0.55, 0.6, 0.65, 0.7, 0.75, 0.8, 0.83, 0.87, 0.9).[61]

In fact, the magnetic properties for the charge ordered manganites should be also affected by phase separations.[29,64] It is expected that the coexistence of FM and AFM phases will lead to an exchange bias (EB), as reported in $La_{1-x}Ca_xMnO_3$ ($0.55 \leq x \leq 0.95$) compound by Huang *et al.*[65] The EB effect generally manifests itself as a shift of the FM hysteresis loop from the zero-field axis due to the exchange coupling at the interface between FM and AFM spin structures.[66] Figure 11 shows the zero-field-cooled (ZFC) and field-cooled (FC, $H_{cool} = 50$ kOe, 1 Oe = 79.5775 A·m$^{-1}$) magnetization–magnetic field ($M$–$H$) loops at 5 K for $La_{1-x}Ca_xMnO_3$ ($0.55 \leq x \leq 0.95$).[65] Figure 11(g) shows the EB field $H_{EB}$ versus the Ca concentration $x$ at 5 K. The $H_{EB}$ is defined as $H_{EB} = |H_1 + H_2|/2$, where $H_1$ and $H_2$ denote the left and right coercivity fields, respectively. The EB effect is clearly related to the FM phases induced by the electronic phase separation in the AFM background for the charge ordered manganites. This intrinsic inhomogeneity-induced EB effect is important for designing related devices.[65]

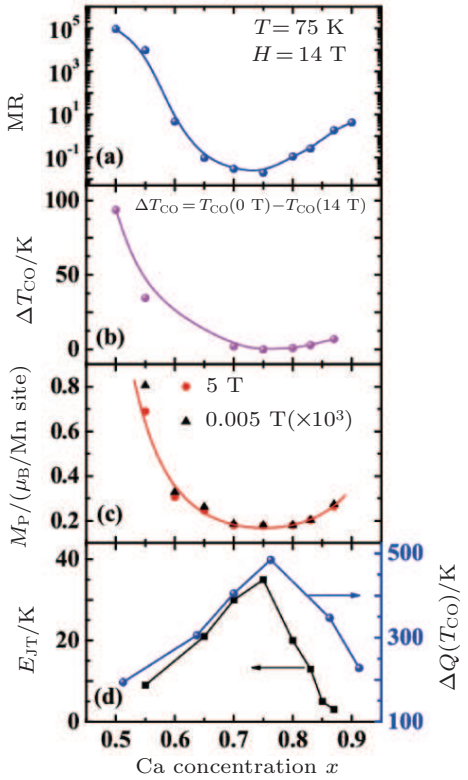



**Fig. 10.** Ca-concentration $x$ dependence of (a) MR at $H = 14$ T and $T = 75$ K, (b) $\Delta T_{CO}$, (c) $M_P$ at $H = 0.005$ T and 5 T, (d) $E_{JT}$ and $\Delta Q(T_{CO})$ for $La_{1-x}Ca_xMnO_3$ ($0.55 \leq x \leq 0.87$).[63]

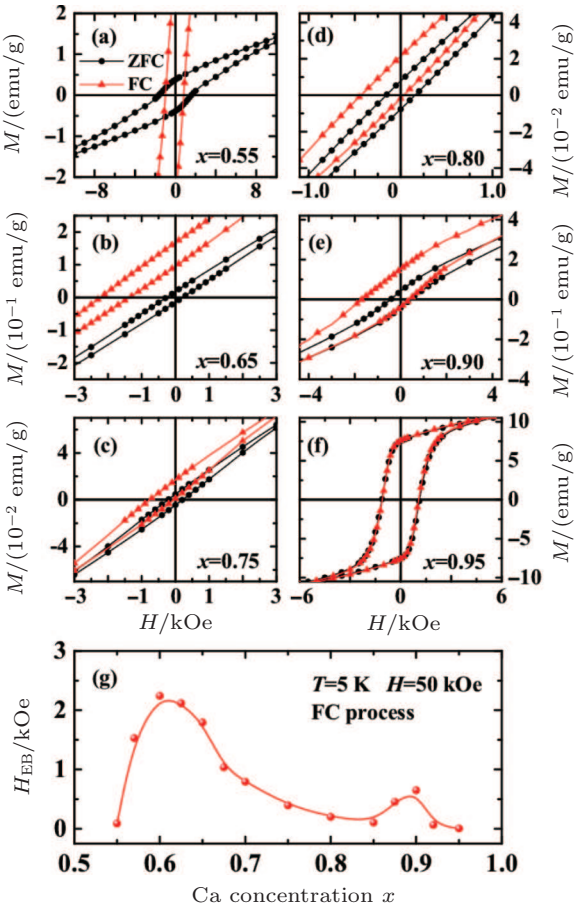



**Fig. 11.** (a)–(f) Typical ZFC and FC $M$–$H$ loops of the $La_{1-x}Ca_xMnO_3$ samples with $0.55 \leq x \leq 0.95$ at 5 K, and (g) Ca concentration $x$ dependencies of $H_{EB}$ at 5 K. Both the measuring and FC fields ($H_{cool}$) are 50 kOe.[65]

## 3. Heterostructure devices

The colossal magnetoresistance effect of perovskite manganites in single phase is one of the outstanding phenomena observed in transition-metal oxides and has stimulated intensive studies for many interesting physical properties associated with competing degrees of freedom of spin, charge, orbital, and lattice.[5] Therefore, various devices were designed by using the rich physics involved in manganites, including hole-doped p-type semiconductivity, complex electronic structure, phase separation, half-metallicity, etc.[5] Several key prototype devices will be introduced here.

### 3.1. p–n junction

As we know, the low level doped $La_{1-x}AE_xMnO_3$ ($AE$ = Ca, Sr, and Ba) manganites always exhibit p-type semiconductivity, which can be used to construct novel p–n junctions with n-type Nb-doped $SrTiO_3$ (SNTO) substrates. The typical temperature-dependent current–voltage ($I$–$V$) curves for manganite/SNTO p–n junctions, taking $La_{0.67}Sr_{0.33}MnO_3$/SNTO as an example, are shown in Fig. 12, presenting a good rectifying behavior where the junction resistance declines significantly with increasing bias. It should be mentioned that these manganite/titanate p–n junctions exhibit magnetically and electrically tunable physical properties due to the rich band structure at the interface of the heterostructures.[16,67–71]

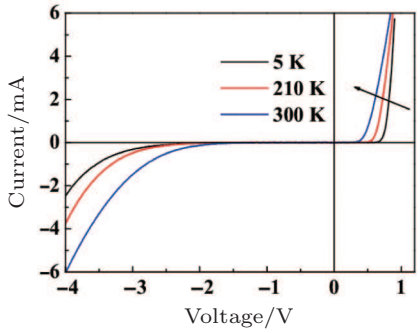



**Fig. 12.** The $I$–$V$ curves of $La_{0.67}Sr_{0.33}MnO_3$/SNTO p–n junction at 5, 210, and 300 K.

#### 3.1.1. Electric field manipulating metal–insulator transition

By taking advantage of "band gap engineering," one can utilize the large changes in both electric and magnetic properties in manganite/titanate p–n junctions.[67,72] In $La_{0.9}Ba_{0.1}MnO_3$/SNTO p–n junction with Nb-0.01 wt% doped $SrTiO_3$, besides a good rectifying effect, the junction property strongly depends on the bias voltage $V_{bias}$, as shown in Fig. 13.[67] At low bias $V_{bias}$ from +0.6 V to +0.8 V, the p–n junction is semiconductive, and the junction resistance monotonously increases with decreasing temperature. However, with further increased bias, a semiconductor–metal transition ($T_p$) in junction resistance–temperature curves appears at $V_{bias} = +1.0$ V, and it increases gradually with increasing $V_{bias}$. Furthermore, this giant electric field-dependent junction resistance differs for junctions with different thicknesses (15 nm, 30 nm) of the $La_{0.9}Ba_{0.1}MnO_3$ layer, as shown in Fig. 13(a),[67] due to the more significant manipulation of carrier density in a thinner $La_{0.9}Ba_{0.1}MnO_3$ film by the carrier injection from n-type materials. Figure 13(b) shows the temperature dependence of magnetoresistance in a magnetic field of 5 T for $La_{0.9}Ba_{0.1}MnO_3$/SNTO with 30-nm $La_{0.9}Ba_{0.1}MnO_3$ at different bias voltages.[67] The junction resistance was reduced by magnetic field in all temperature ranges, and the MR $[(R_{junction}(H = 0\ T) - R_{junction}(H = 5\ T)]/R_{junction}(H = 0\ T) \times 100\%)$ increases monotonically with decreasing temperature and bias. The semiconductor–metal trasnsition and magnetoresistance manipulated by low bias voltage in manganite/titanate p–n junction indicate the double exchange ferromagnetism in manganite can be switched by electric fields.[67]

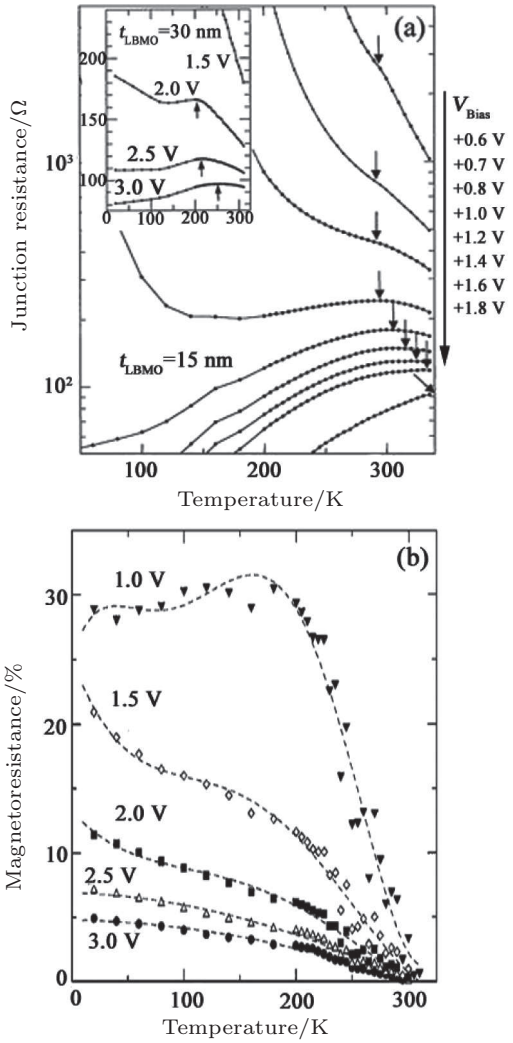



**Fig. 13.** (a) Temperature dependencies of junction resistances of an $La_{0.9}Ba_{0.1}MnO_3$ (15 nm)/SNTO heterojunction measured under various bias voltages. The arrows indicate metal–insulator transition temperatures. The inset shows that of $t_{LBMO} = 30$ nm. (b) Temperature dependence of magnetoresistance ($H = 5$ T) measured under various bias voltages of the $La_{0.9}Ba_{0.1}MnO_3$/SNTO heterojunction ($t_{LBMO} = 30$ nm). The MR ratio is defined as $(R_{junction}(H = 0\ T) - R_{junction}(H = 5\ T))/R_{junction}(H = 0\ T) \times 100\%$.[67]

### 3.1.2. Positive magnetoresistance

It is interesting that both negative MR and positive MR effects can be observed in the manganite/titanate junctions.[16,70,71,73,74] Figure 14 shows magnetic field dependencies of MR for $La_{0.82}Ca_{0.18}MnO_3$/SNTO p–n junction at 60, 90, 180, and 240 K. It can be seen that the MR is always negative within the whole measured temperature range at a small bias current ($I = 3$ μA), and it is still negative at 60 K and 90 K at a larger bias current ($I = 300$ μA) but becomes positive at 180 K and 240 K. While only negative MR is observed for the $La_{0.7}Ca_{0.3}MnO_3$/SNTO p–n junction.[16,75] Similar manipulations of MR from negative to positive were also reported in the $La_{0.7}Ce_{0.3}MnO_3$/SNTO p–n junction,[71] the $La_{0.32}Pr_{0.35}Sr_{0.33}MnO_3$/SNTO p–n junction,[73] the $SrTiO_{3-\delta}/La_{0.9}Sr_{0.1}MnO_3/SrTiO_{3-\delta}/La_{0.9}Sr_{0.1}MnO_3$ (n–p–n–p) heterojunctions,[76] etc. The results mentioned above indicate that the negative and positive MR in manganite/SNTO do not depend only on temperature and bias current, but also depend on the carrier concentration, which is directly related to the band structure at the p–n interface.[16,75]

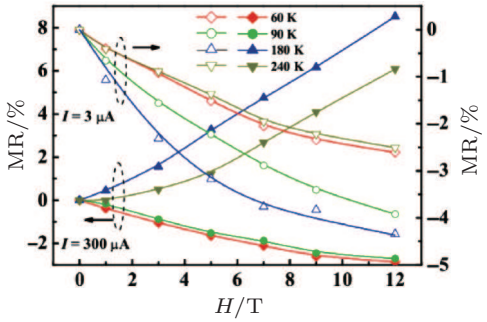



**Fig. 14.** Magnetic field dependence of MR at 60, 90, 180, and 240 K for two different bias currents $I = 3$ μA (open symbols) and 300 μA (closed symbols) for the $La_{0.82}Ca_{0.18}MnO_3$/SNTO p–n junction.[16]

As discussed with respect to Fig. 3, the Fermi surface lies in the $e_g^{1\uparrow}$ band, and the $e_g^{2\uparrow}$ and $t_{2g}^{\downarrow}$ bands are above the Fermi level and near it. Therefore, as the electric field applied across the p–n junction increases, the electrons injected from SNTO into the manganite will occupy these empty bands from low to high. When the electrons injected from SNTO to $La_{0.82}Ca_{0.18}MnO_3$ predominantly occupy the $e_g^{1\uparrow}$ ($e_g^{2\uparrow}$) band, the injected carriers are of majority spin direction (up) and the junction retains its negative MR. However, when the spin orientation of $t_{2g}^{\downarrow}$ is antiparallel to the majority spin direction, the electrons from SNTO occupy the $t_{2g}^{\downarrow}$ band and increasing the magnetic field will increase the spin scattering in the $t_{2g}^{\downarrow}$ band, resulting in a positive MR.[16,75]

By selecting proper dopant composition in manganites, one can achieve a large MR effect in manganite/SNTO p–n heterojunctions at low magnetic field and high temperature, which is more suitable for spintronic applications than the CMR effect in single phase at high magnetic field. Figure 15 shows the negative bias voltage dependence of the positive MR (MR = $R(H)/R(0) - 1$) in $La_{0.9}Sr_{0.1}MnO_3$/SNTO p–n heterojunction.[70] In 5 Oe, a positive MR value of 10.6% at 290 K can be obtained.

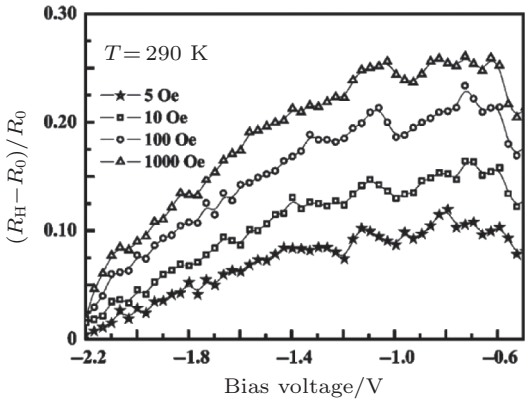



**Fig. 15.** The variation of MR values of $La_{0.9}Sr_{0.1}MnO_3$/SNTO p–n heterojunction with the negative bias voltage at different magnetic fields at 290 K.[70]

## 3.2. Magnetoelectric coupling devices

### 3.2.1. Ferroelectric controlled electric and magnetic properties of manganites

Due to the sensitivity of the spin, charge, orbital, and lattice degrees of freedom to external stimulus in manganites, the magnetic and electric properties of manganites can be tuned *in situ* by using a neighboring ferroelectric substance through strain and/or charge manipulation in the manganites/ferroelectric multiferroic heterostructures.[31,51,77,78] The ferroelectric materials $(1-x)Pb(Mg_{1/3}Nb_{2/3})O_3 - xPbTiO_3$ (PMN-PT) with composition near the morphotropic phase boundary ($x = 0.33$) exhibit outstanding piezoelectric activity and giant remanent polarization, and can be used as ferroelectric substrates to grow manganite thin films.[77,79–85] Figures 16(a) and 16(b) show typical butterfly-like strain–electric field hysteresis loops and rectangle-like polarization-electric field loops of PMN-PT single crystals. Figures 16(c) and 16(d) show the strain and ferroelectric field effects on the resistances of the $Pr_{0.5}Ca_{0.5}MnO_3$ film in $Pr_{0.5}Ca_{0.5}MnO_3$/PMN-PT heterostructures at different temperatures.[86] A roughly symmetrical butterfly-like resistance–electric field ($R$–$E$) hysteresis loop at 296 K is a typical behavior of the resistance modification due to the polarization-rotation-induced strain in the PMN-PT substrate. The strain-induced resistance manipulation implies that the intrinsic double-exchange interaction is strongly influenced by the in-plane strain.[87] With temperature decreasing to 180 K (Fig. 16(d)), the rectangular-like $R$–$E$ loop appears, indicating an enhanced ferroelectric field effect with decreasing temperature in $Pr_{0.5}Ca_{0.5}MnO_3$/PMN-PT heterostructures. Thus one can control the properties of manganites by electric voltage in manganite/ferroelectric heterojunctions, due to the transfer of electric-field-induced strain to the manganite and the modification of the charge carrier density of the manganite by ferroelectric fields.

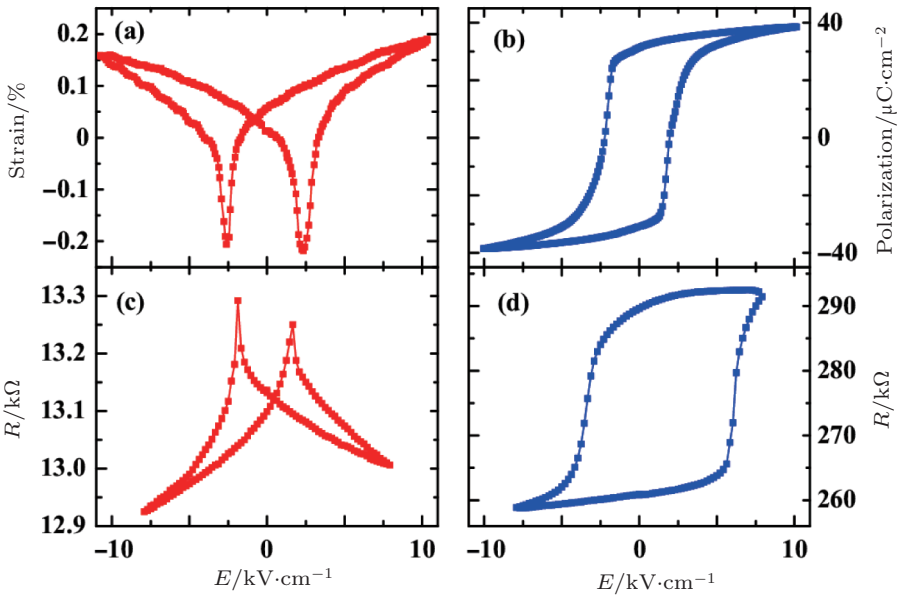



**Fig. 16.** Typical (a) butterfly-like strain–electric field and (b) rectangle-like polarization-electric field hysteresis loops of PMN-PT single crystals at room temperature. Changes in the resistance of the $Pr_{0.5}Ca_{0.5}MnO_3$ film at (c) 296 K and (d) 180 K as a function of bipolar electric field applied to the substrate.[86]

Recently, Yang *et al.* reported controlling anisotropic magnetic properties by means of anisotropic strain effects.[88] They found that the remanent magnetization of $La_{2/3}Sr_{1/3}MnO_3$ along [100] direction was suppressed through a strain effect, while along $[01\bar{1}]$ it was enhanced for film deposited on (011) PMN-PT single substrate. The tunability of the remanent magnetization along the [100] and $[01\bar{1}]$ directions is about $-17.9\%$ and $+157\%$, respectively, in electric field of $+7.27$ kV/cm.[88] This large anisotropic remanent magnetization tunability may find potential applications in electrically written and magnetically read memories.[89] Likewise, the valence state of Mn induced by electronic charge manipulation through field effect was observed in $Pb(Zr_{0.2}Ti_{0.8})O_3/La_{0.8}Sr_{0.2}MnO_3$ multiferroic heterostructure, resulting in the switching of magnetism in $La_{0.8}Sr_{0.2}MnO_3$ with the electric field "on" and "off," giving rise to a large magnetoelectric coupling effect.[90,91]

Besides the strain and field effects, Yu *et al.* found that electronic orbital reconstruction at the manganite/ferroelectric interface directly influences the coupling between $La_{0.7}Sr_{0.3}MnO_3$ and $BiFeO_3$ and results in the pinned uncompensated spins required for exchange bias (EB).[92] This EB can be controlled by electric fields, where two distinct exchange-bias states can be reversibly switched by the ferroelectric polarization of $BiFeO_3$.[93]

### 3.2.2. Magnetic field effects on the magnetoelectric coupling in manganite/ferroelectric heterostructures

In fact, the magnetoelectric coupling effect can be impacted by both electric and magnetic fields.[30,94] A colossal magnetocapacitance (MC = $[\varepsilon(H) - \varepsilon(0)]/\varepsilon(0)$, where $\varepsilon(H)$ and $\varepsilon(0)$ are the dielectric constants with and without magnetic fields) up to 1100% near the Curie temperature $T_C = 220$ K of $La_{5/8}Ca_{3/8}MnO_3$ has been observed in the $BiFeO_3/La_{5/8}Ca_{3/8}MnO_3$ heterostructure.[78] (see Fig. 17), which is three orders of magnitude higher than that reported in a single phase $BiFeO_3$ system.[95,96] The colossal magnetocapacitance effect can be achieved in a wide frequency region from 200 kHz to 2 MHz and a wide temperature range from 190 K to 260 K.

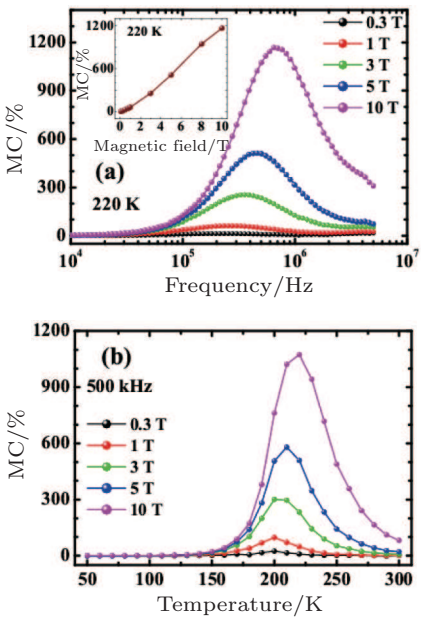



**Fig. 17.** Frequency dependencies of the MC effect at 220 K. The inset shows the magnetic field dependence of maximum MC value at 220 K. (b) Temperature dependencies of the MC effect at a frequency of 500 kHz in magnetic fields up to 10 T.[78]

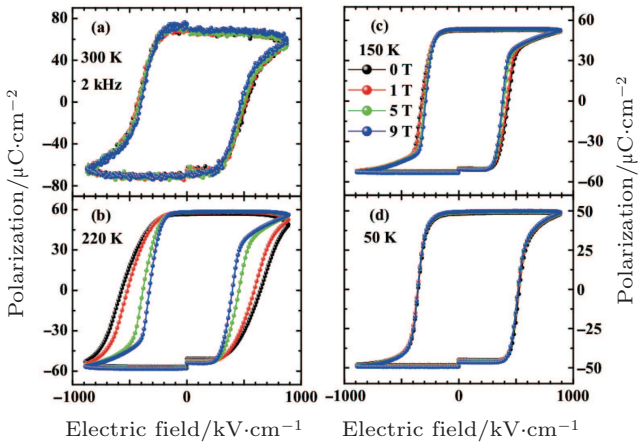



**Fig. 18.** Remanent ferroelectric hysteresis loops of $BiFeO_3/La_{5/8}Ca_{3/8}MnO_3$ at $f = 2$ kHz in magnetic fields of 0, 1, 5, and 9 T at different temperatures: (a) $T = 300$ K, (b) $T = 220$ K, (c) $T = 150$ K, and (d) $T = 50$ K.[51]

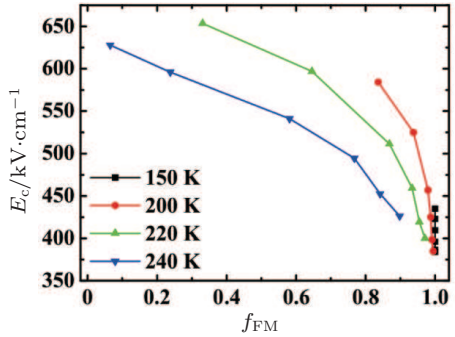



**Fig. 19.** FM volume fraction $f_{FM}$ dependencies of apparent coercive electric field $E_c$ in $La_{5/8}Ca_{3/8}MnO_3$.[51]

Figure 18 shows the temperature and magnetic field dependencies of the remanent ferroelectric hysteresis loops for epitaxial $BiFeO_3/La_{5/8}Ca_{3/8}MnO_3$ film.[51] With increasing magnetic field, the room-temperature polarization has little response to magnetic field (Fig. 18(a)), and no obvious differences in the *P*–*E* hysteresis loops are observed at temperatures far below the ferromagnetic transition temperature $T_C \sim 220$ K of $La_{5/8}Ca_{3/8}MnO_3$ (Figs. 18(c) and 18(d)). However, in the temperature range near $T_C$, the values of the apparent coercive electric field $E_c$ gradually decrease with increasing magnetic fields, as shown in Fig. 18(b). Based on the phase-separation model discussed in Subsection 2.1,[46] it is found that $E_c$ decreases rapidly with increasing ferromagnetic volume fraction $f_{FM}$ of $La_{5/8}Ca_{3/8}MnO_3$, especially as $f_{FM}$ gets close to 1 near 220 K, as shown in Fig. 19,[51] which reflects the effect of $La_{5/8}Ca_{3/8}MnO_3$ phase separation on the magnetoelectric coupling of the interface between $BiFeO_3$ and $La_{5/8}Ca_{3/8}MnO_3$. Through analyzing the frequency dependencies of the impedance module $|Z|$ of $BiFeO_3/La_{5/8}Ca_{3/8}MnO_3$ heterostructure, $BiFeO_3$ and $La_{5/8}Ca_{3/8}MnO_3$ in different temperatures and magnetic fields, Liu *et al.* found that the notable decrease of the apparent coercive field $E_c$ with increasing magnetic field around $T_C$ is closely related to the voltage drops across the $La_{5/8}Ca_{3/8}MnO_3$ layer and the magnetoelectric-coupled interface between $BiFeO_3$ and $La_{5/8}Ca_{3/8}MnO_3$, which can be influenced by magnetic fields due to the phase separation in $La_{5/8}Ca_{3/8}MnO_3$.[51]

### 3.3. Spintronic devices based on half-metallic property in manganites

#### 3.3.1. High TMR effect in magnetic tunnel junction

The CMR effect in both bulk and single film always needs a large magnetic field, which limits its application in spintronic devices.[8] Therefore, alternative devices were designed to overcome this obstacle, such as magnetic tunnel junctions (MTJ) that take advantage of the high spin polarization in FM manganites below the Curie temperature.[17,97–99] A magnetic tunnel junction is composed of two ferromagnetic layers (CMR materials) separated by an ultrathin insulating barrier.[17,97,100–102] Because these tunnel junction devices allow true on-off operation, they are very suitable for nonvolatile memory devices such as magnetic random access memories (MRAM). This device was first realized in the $La_{0.67}Sr_{0.33}MnO_3/SrTiO_3/La_{0.67}Sr_{0.33}MnO_3$ (LSMO/STO/LSMO) junction with tunneling magnetoresistance (TMR) of 86% at 4.6 K.[32] Obata *et al.* fabricated LSMO/STO/LSMO junctions with a thin STO tunnel barrier[100] and found that TMR disappears above 200 K for a junction with STO thickness $t_{STO} = 2.4$ nm, whereas for a thinner junction ($t_{STO} = 1.6$ nm) the TMR value was still observed up to 270 K. Furthermore, an extremely large TMR response up to 1800% was obtained in an LSMO/STO/LSMO/Co/Au device, as shown in Fig. 20, where the spin-polarization of LSMO at the interface with STO can reach at least 95%.[97] However, when the spin-polarizations of the two ferromagnetic electrodes have opposite signs, an inverse TMR is observed with a smaller resistance in the antiparallel configuration, such as in LSMO/I/Co junctions, where I is an insulating barrier of STO, $Al_2O_3$, or $Ce_{0.69}La_{0.31}O_{1.845}$.[102] An unexpected result is the fact that the sign of TMR depends on the nature of the insulating barrier: a maximum tunneling current is observed in a parallel configuration with $Al_2O_3$, whereas with STO, an inverse TMR corresponding to a maximum tunneling current is observed for an antiparallel configuration.[102] Interestingly, in all-manganite tunnel junctions with $La_{0.7}Ca_{0.3}MnO_3$ as ferromagnetic electrodes and $La_{0.3}Ca_{0.7}MnO_3$ with a charge-ordered insulator below 260 K as the tunnel barrier, a large TMR up to 500% at 6 K has been observed, wherein it is found that the response of this junction is determined not only by the high spin-polarization of FM electrodes but also by novel interface-induced phases.[103] These results confirm that the metal–oxide interfaces play an important role in MTJ devices.

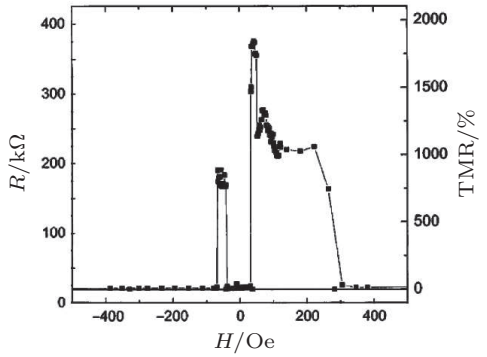



**Fig. 20.** Magnetic field dependence of the junction resistance for LSMO/STO/LSMO/Co/Au device at 4.2 K.[97]

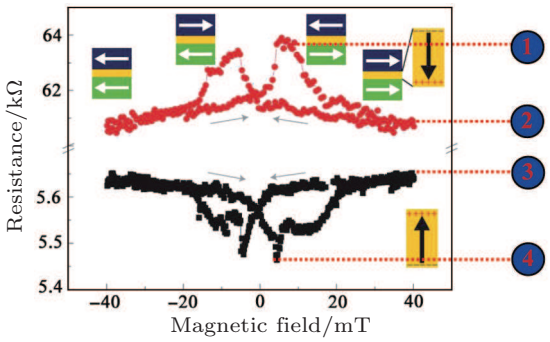



**Fig. 21.** Resistance versus magnetic field curves for a Co/PZT (3.2 nm)/LSMO junction measured at 50 K with the ferroelectric polarization pointing upward (black curve) and downward (red curve).[115]

### 3.3.2. Four states and magnetoelectric coupling in MFTJ

Besides the TMR phenomena in MTJ mentioned above, the functionality of a tunnel junction can be enhanced by employing a ferroelectric material as the barrier layer. Recently, it has been theoretically[104–106] and experimentally[107–109] demonstrated that the tunneling conductance through a ferroelectric barrier depends on the polarization direction of the barrier, i.e., a tunneling electroresistance (TER) effect. Therefore, combining an MTJ with a ferroelectric barrier, producing a multiferroic tunnel junction (MFTJ), will add new functionalities to the MTJ and make the junction resistance sensitive not only to the magnetization alignment of the ferromagnetic electrodes but also to the polarization of the ferroelectric barrier.[110,111] This makes an MFTJ device display four non-volatile resistance states due to the coexistence of TMR and TER effects. It is also a magnetoelectric device cross-controlled by magnetic and electric fields, owing to the interfacial magnetoelectric coupling effect. Recently, such ferromagnetic/ferroelectric/ferromagnetic MFTJs with four non-volatile resistance states and magnetoelectric coupling were experimentally fabricated and investigated in Fe (or Co)/$BaTiO_3$/$La_{0.7}Sr_{0.3}MnO_3$,[112,113] $La_{0.4}Sr_{0.3}MnO_3$/$BiFeO_3$/$La_{0.7}Sr_{0.3}MnO_3$,[114] and Co/$PbZr_{0.2}Ti_{0.8}O_3$/$La_{0.7}Sr_{0.3}MnO_3$[115] MFTJs.

Figure 21 shows the resistance versus magnetic field curves for a Co/PZT(3.2 nm)/LSMO junction, which exhibits both a TMR effect due to the ferromagnetic electrodes and a TER effect driven by the switching of the ferroelectric polarization of the barrier,[115] reflecting the four distinct resistance states obtained. In addition, it is noted that the switching of the ferroelectric polarization can also invert the sign of the spin polarization at the Co/PZT interface and lead to different signs of TMR at two polarization states. The magnetoelectric coupling at such a multiferroic interface could be due to hybridization at the interface, charge carrier doping, or spin-dependent screening in the magnetic electrodes.[115]

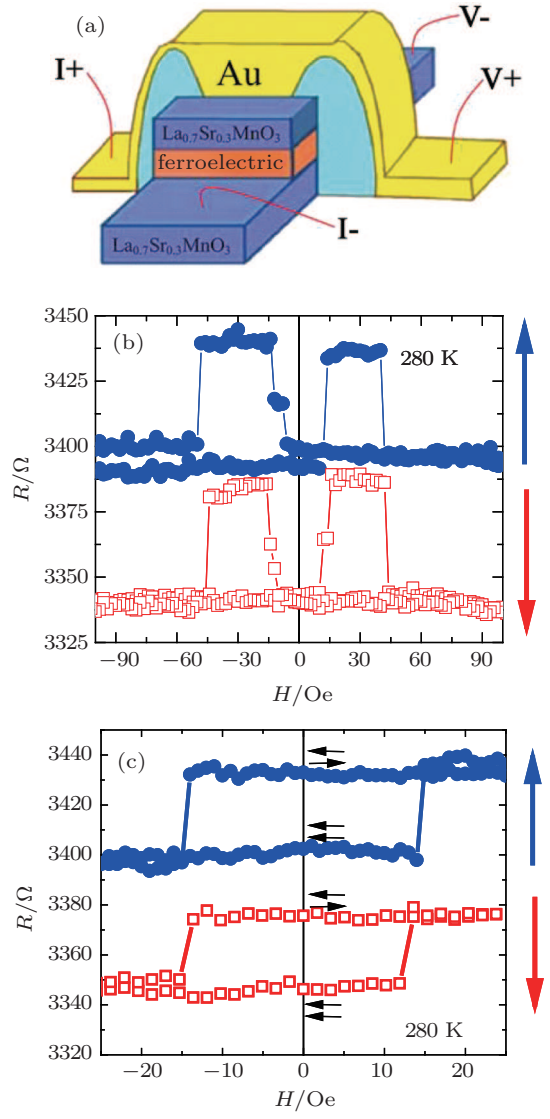



**Fig. 22.** (a) Schematic diagram of MFTJ device geometry. Resistance $R$ versus $H$ loops between (a) ±100 Oe and (b) ±30 Oe for an $La_{0.7}Sr_{0.3}MnO_3$/$Ba_{0.95}Sr_{0.05}TiO_3$/$La_{0.7}Sr_{0.3}MnO_3$ MFTJ measured at 10 mV and 280 K after poling the ferroelectricity upward (red) and downward (blue). Horizontal arrows indicate the direction of electrode magnetization and vertical arrows indicate the direction of barrier polarization.[116]

Using half-metallic manganite $La_{0.7}Sr_{0.3}MnO_3$as ferromagnetic electrodes and nanometers-thick (Ba, Sr)$TiO_3$

as ferroelectric barrier, Yin *et al.* have studied all-perovskite MFTJs as schematically shown in Fig. 22(a), and observed four non-volatile states at room temperature, which demonstrates the junctions' application potential.[116–118] As shown in Fig. 22(b), the magnetic field dependence of the junction resistance for an $La_{0.7}Sr_{0.3}MnO_3/Ba_{0.95}Sr_{0.05}TiO_3/La_{0.7}Sr_{0.3}MnO_3$ MFTJ was measured after aligning the ferroelectric polarization of $Ba_{0.95}Sr_{0.05}TiO_3$ barrier downward (by $+1.5$ V poling voltage) or upward (by $-1.5$ V poling voltage).[116] It can be seen that the entire *R–H* curve shifts after reversing the polarization of the barrier so that both parallel and antiparallel resistances are switched to different values and four resistance states are observed. Standard MTJ memory loops can also be obtained for both polarization states and the resistance can be switched from one memory loop to another by reversing the ferroelectricity of the barrier, as shown in Fig. 22(c). In other words, these non-volatile junction resistances between the two polarization states can be switched each other directly by reversing the barrier polarization repeatedly, as shown in Fig. 23. Here, the red and blue dots mean that the switching was observed between parallel and antiparallel magnetic states [reached by *R–H* sweep (see Fig. 23)], respectively. Hence, after applying positive and negative voltages, two parallel and two antiparallel states, i.e., a distinct four-state prototype device was realized at room temperature.

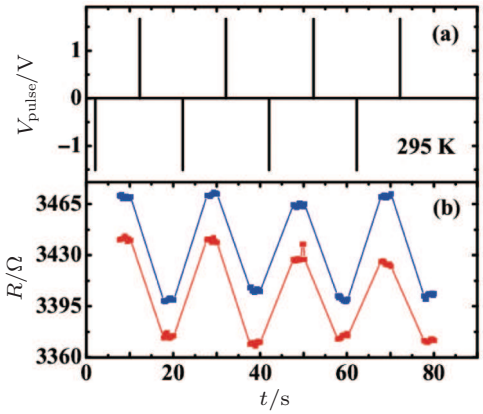



**Fig. 23.** In response to (a) the applied voltage pulses, (b) switching of the junction resistance (measured at 10 μA) for an $La_{0.7}Sr_{0.3}MnO_3/Ba_{0.95}Sr_{0.05}TiO_3/La_{0.7}Sr_{0.3}MnO_3$ MFTJ at parallel (red) and antiparallel (blue) states.[116]

In an MFTJ, an interfacial magnetoelectric effect will show up at ferroelectric/ferromagnetic interface due to chemical bonding, spin-dependent screening, etc., therefore, the magnetization can be manipulated by electric field through switchable ferroelectric polarization.[119,120] Based on the intrinsic relationship between charge and magnetism in doped manganites $La_{1-x}A_xMnO_3$ ($A$ = Ca, Sr, or Ba), all of which exhibit rich phase diagrams as a function of hole concentration $x$,[7] the carrier density of $La_{1-x}A_xMnO_3$ near the interface with a ferroelectric material can be effectively altered by the screening charges and will result in another kind of ferroelectric control of magnetism in $La_{1-x}A_xMnO_3$.[31,90,121]

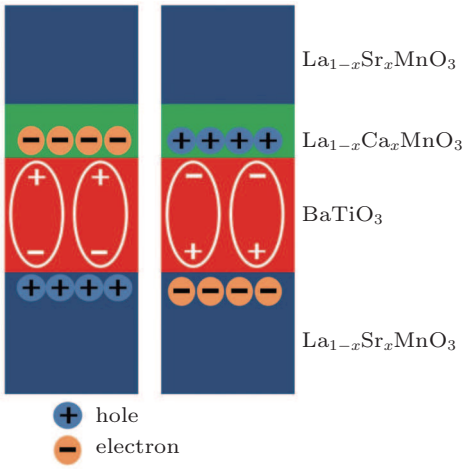



**Fig. 24.** Schematic demonstration of the screening charge accumulation in electrodes for opposite ferroelectric polarization orientations in the BTO layer.[122]

Very recently, using first-principles density-functional calculations, Burton and Tsymbal[123] predicted that a giant TER effect could be obtained by exploiting a magnetoelectric interaction between a ferroelectric $BaTiO_3$ tunneling barrier and a magnetic $La_{1-x}Sr_xMnO_3$ electrode. According to this theory, Yin *et al.* then designed and fabricated[122] epitaxial $La_{0.7}Sr_{0.3}MnO_3/BaTiO_3/La_{0.5}Ca_{0.5}MnO_3/La_{0.7}Sr_{0.3}MnO_3$ (50 nm)/(3 nm)/(0.4 nm–1.2 nm)/(30 nm) (bottom/barrier/top) tunnel junctions with a thin $La_{0.5}Ca_{0.5}MnO_3$ film inserted between the ferromagnetic $La_{0.7}Sr_{0.3}MnO_3$ electrode and ferroelectric $BaTiO_3$ barrier. On one hand, for polarizing the thin $La_{0.5}Ca_{0.5}MnO_3$ layer (see Fig. 24), the screening electron accumulation or hole depletion will change the doping level of $La_{0.5}Ca_{0.5}MnO_3$ to $x < 0.5$, which is in ferromagnetic metallic phase. While at the other side of the $BaTiO_3$ barrier, because the stoichiometry of $La_{0.7}Sr_{0.3}MnO_3$ is far enough away from the phase boundary, the theoretical calculation predicted that the magnetic reconstruction will not occur.[124] On the other hand, for polarization pointing away from the $La_{0.5}Ca_{0.5}MnO_3$ film, the electron depletion or hole accumulation will change $La_{0.5}Ca_{0.5}MnO_3$ to $x > 0.5$, pushing it into antiferromagnetic insulating phase. A few unit-cells of antiferromagnetic $La_{0.5}Ca_{0.5}MnO_3$ may act as an atomic-scale spin valve by filtering spin-dependent current and increasing the junction resistance as well. In addition, the metallicity change of $La_{0.5}Ca_{0.5}MnO_3$ into insulation along [001] crystal direction will effectively increase the barrier thickness and reduce the tunneling conductance significantly. Thus, a much larger TER effect can be obtained.

Figure 25(a) shows the resistance memory loops as a function of pulsed poling voltage for an MFTJ with two unit cells $La_{0.5}Ca_{0.5}MnO_3$ inserted, labeled as S1. Each datum point in the hysteresis curve is tested at a fixed voltage bias

10 mV after applying a voltage pulse. The resistance is higher when a large enough positive voltage is applied to polarize the ferroelectricity downward, and switches to a lower resistance state when ferroelectricity is reversed by a large enough negative voltage bias. This is consistent with our design that the negative voltage will switch the ferroelectricity upward, pointing to the $La_{0.5}Ca_{0.5}MnO_3$ that will create a hole depletion as illustrated in Fig. 24. This will push $La_{0.5}Ca_{0.5}MnO_3$ into a more ferromagnetic metallic phase. The TER ratio reaches up to $\sim 5 \times 10^3\%$ and is much larger than the previously reported MFTJs in trilayer patterned junctions.[112–114,116,117,125] For comparison, the $R$–$V_{\rm pulse}$ loop of another junction without $La_{0.5}Ca_{0.5}MnO_3$, labeled S2, was also measured and shown in Fig. 25(b). The TER ratio for this junction is only $\sim 30\%$, much smaller than for S1.

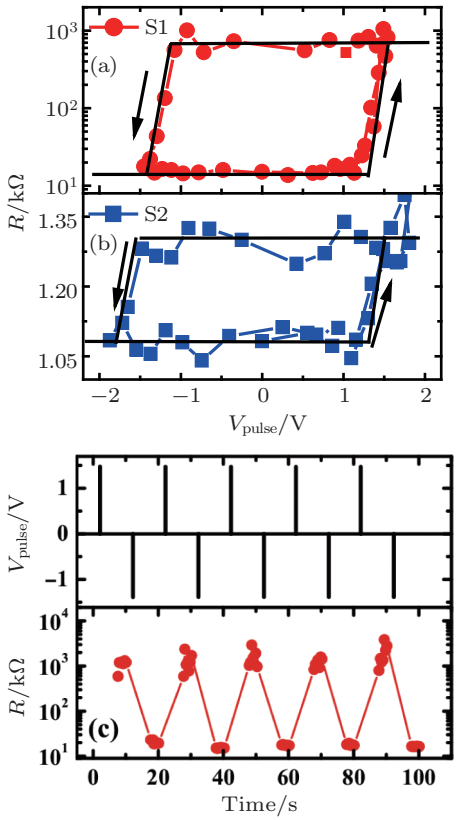



**Fig. 25.** (a) and (b) Resistance memory loops as a function of pulsed poling voltage ($V_{\rm pulse}$) at 40 K for MFTJs with (a) and without (b) $La_{0.5}Ca_{0.5}MnO_3$ inserted. The solid lines are a guide to the eyes. The arrows indicate the direction of pulse sequence. (c) Applied voltage pulse train (top panel) and the corresponding resistance switching (bottom panel) between positive and negative polarization states for S1 at 5 K and 10 mV.[122]

Besides the large magnitude of the TER ratio, the reproducibility of polarization states is a decisive characteristic of an MFTJ for a memory device. The resistance states of S1 can be switched between positive and negative polarization states reproducibly. As shown in Fig. 25(c), through a series of consecutive switching of the barrier polarization by voltage pulses ($\pm$1.4 V), the resistance at 10 mV bias switches back and forth between two resistance states repeatedly and the TER value is as large as $\sim 8 \times 10^3\%$. The switching between two polarization states has been measured several hundred times at different temperatures and biases, and a large and reproducible TER effect can be observed accordingly, suggesting possible applications in nondestructive readout of polarization direction.[122]

### 3.3.3. Spin detector in organic spin-valves

Recently, the long spin relaxation time of organic semiconductors has attracted much attention in the spintronics community. The organic spin-valve (OSV) is a device based on an organic semiconductor sandwiched between $La_{2/3}Sr_{1/3}MnO_3$ (LSMO) and metal electrodes. A larger spin-valve magnetoresistance effect that was discovered in the sandwich structures is associated with exotic properties of the magnetic electrode and organic semiconductors with long spin lifetimes.[98] It should be pointed out that although the organic spacers in OSVs are composed of light elements having weak spin–orbital interaction and consequently possessing long spin-relaxation times,[126] the hyperfine interaction (HFI) has an important role in organic magnetotransport.[127] The role of the HFI in OSVs, by replacing hydrogen atoms ($^1$H, nuclear spin $I = 1/2$) in the organic $\pi$-conjugated polymer poly (dioctyloxy) phenylenevinylene (DOO-PPV) spacer (dubbed here H-polymer) with deuterium atoms ($^2$H, $I = 1$) (hereafter D-polymer) having a much smaller HFI constant $\alpha$, specifically $\alpha(\mathrm{D}) = \alpha(\mathrm{H})/6.5$, has been investigated with LSMO and Co as two ferromagnetic electrodes.[128] Figure 26 shows the magnetoresistance hysteresis loops for two similar OSVs with the organic layer thickness $\sim 25$ nm based on H- and D-polymers (devices a and b, respectively) at $T = 10$ K and $V = 10$ mV. It can be seen that the prototype devices based on the D-polymer show much larger MR values than those based on the H-polymer. Nguyen *et al.* found that the spin-diffusion length $\lambda_{\rm s}$ for D-polymers OSV is $\lambda_{\rm s}(\mathrm{D}) = 49$ nm, whereas $\lambda_s(\mathrm{H}) = 16$ nm, which contributes to the better magnetic properties of the D-polymer-sandwiched OSVs.[128] A similar isotope effect on magnetoresistance is observed in $Alq_3$-based OSVs.[129] However, it should be noted that not all organic semiconductors show a strong isotope effect,[130] presumably because interactions other than HFI dominate the polaron-pair spin Hamiltonian[128] in a specific organic semiconductor, such as triplet-polaron interaction or/and spin–orbit coupling.

With the buckeyball $C_{60}$ molecule as the organic semiconductor spacer in OSVs, a 7% MR at $V = 100$ mV and $T = 10$ K is obtained, as shown in Fig. 27(a).[131] Surprisingly, it is found that the MR of $C_{60}$-based OSVs first increases as the interlayer $C_{60}$ thickness $d$ increases, reaches a maximum near $d_0 = 35$ nm, then exponentially decreases with $d$, as shown in Fig. 27(b).[131] This is related to the $C_{60}$ film

crystallinity, which increases with $d$ below $\sim 45$ nm and saturates near 45 nm. The less disordered $C_{60}$ layer leads to higher charge carrier mobility and a longer spin diffusion length $\lambda_{C_{60}}$ of $C_{60}$, thus resulting in larger MR.[131] Further increasing $d$ will diffuse more spins and consequently reduce the MR.

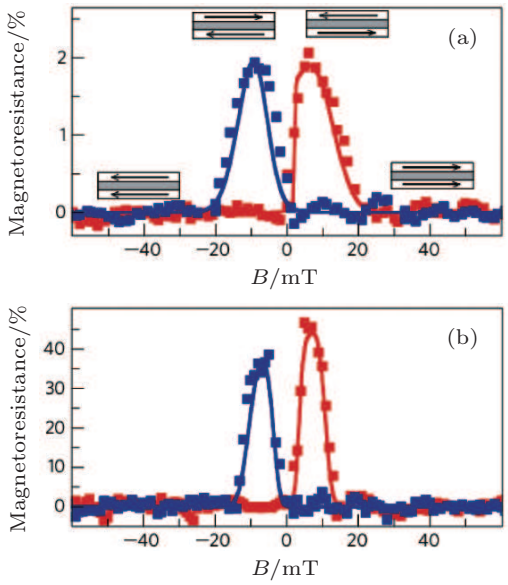



**Fig. 26.** Isotope dependence of the magnetoresistance response in OSVs based on DOO-PPV polymers. Magnetoresistance loop of LSMO(200 nm)/DOO-PPV(25 nm)/Co(15 nm) spin-valve devices based on H- (a) and D- (b) polymers measured at $T = 10$ K and $V = 10$ mV, respectively.[128]

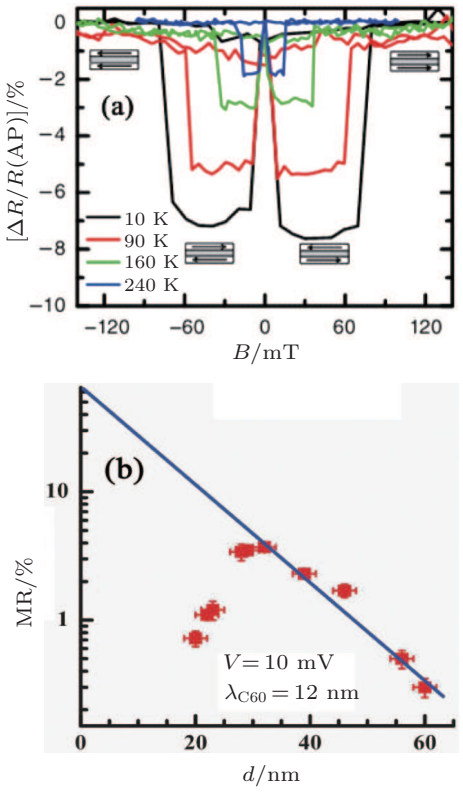



**Fig. 27.** (a) MR of $C_{60}$-based OSVs measured at $V = 100$ mV and different temperatures with $d = 35$ nm. (b) $C_{60}$-thickness dependence of MR at $V = 10$ mV and $T = 10$ K.[131]

## 4. Nanosized manganite particles

### 4.1. Particle size effect on the magnetic properties of $La_{0.6}Pb_{0.4}MnO_3$

In the past few years, much attention has been drawn toward nanocrystalline CMR materials because when the size of these materials is reduced to nanometer scale, they exhibit a number of unique properties unlike their bulk properties, such as low-field high magnetoresistance effect,[132,133] superparamagnetism,[134] and surface spin-glass.[135,136]

As for the ferromagnetic manganites, the effects of the nanoparticles' size on the magnetic properties and the origin of these effects are controversial issues.[137–139] Mahesh *et al.* reported that the $T_C$ of $La_{0.7}Ca_{0.3}MnO_3$ and $La_{0.7}Sr_{0.3}MnO_3$ nanoparticles decreases significantly with decreasing particle size.[137] However, Zheng *et al.* found that the metal–insulator transition temperature $T_{Rmaxis}$ of the $La_{0.67}Ca_{0.33}MnO_3$ markedly decreases with decreasing grain size, while the $T_C$ is not sensitive to the grain size.[138] While Dutta *et al.* found that the $T_C$ of $La_{0.875}Sr_{0.125}MnO_3$ nanoparticles increases with decreasing particle size and attributed this to domain status and to the fact that the Mn–O–Mn bond angle and the Mn–O bond length differ from those attributes of bulk samples.[139,140] The $T_C$ of $La_{0.67}Ca_{0.33}MnO_3$ nanoparticles has also been found to increase with decreasing particle size.[139,140]

Recently, Zhang *et al.* systemically studied the effects of particle size on the structural and magnetic properties of ferromagnetic $La_{0.6}Pb_{0.4}MnO_3$ compounds with particle diameters $D$ varying from 5 nm to 100 nm.[141] They found that the ferromagnetic transition temperature $T_C$ clearly decreases with decreasing $D$, as shown in Fig. 28(a). The particle size-dependence of $T_C$ can be described by an empirical formula,

$$T_C(D) = T_{C0}(1 - D_S/D)^{\gamma} \quad (D > D_S), \tag{6}$$

where $T_{C0} = 360$ K is the ferromagnetic transition temperature of the corresponding bulk material, $D_S = 5.8$ nm is the particles' upper limit for the appearance of superparamagnetism, and $\gamma = 0.68$ is the fitting parameter. According to the double exchange model, $T_C$ is closely related to the magnitude of the O-2p-like bandwidth $W_{O_{2p}}$, and the particle size-dependence of $W_{O_{2p}}$ can be expressed as

$$W_{O_{2p}} \propto \cos\omega / d_{Mn-O}^{3.5}, \tag{7}$$

where $\omega = (\pi - \theta_{Mn-O-Mn})/2$ is the tilt angle in the plane of the bond,[142] $\theta_{Mn-O-Mn}$ is the Mn–O–Mn bond angle, and $d_{Mn-O}$ is the Mn–O bond length, which can be obtained from X-ray diffraction refinement.[141] From Fig. 28(a), one can see that the relative value of $W_{O_{2p}}$ decreases with decreasing $D$. The decrease of $W_{O_{2p}}$ will result in the decrease of ferromagnetic transition temperature $T_C$, as depicted in the inset of Fig. 28(a).

The broken exchange bonds and the increasing contribution of the surface effect with decreasing $D$ lead to a decrease of the saturated magnetization $M_S$, as shown in Fig. 28(b).[141] While with decreasing $D$ the magnetic coercive field $H_C$ first increases and reaches a maximum of 295 Oe for the 25-nm sample, then decreases. The variation of $H_C$ is closely related to the evolution of magnetic domain states with particle size.[143] For $D > 25$ nm the $La_{0.6}Pb_{0.4}MnO_3$ nanoparticles have a multidomain structure; while for 5.8 nm$< D \leq 25$ nm the samples seem to have a single domain structure, and for particle sizes less than 5.8 nm, the samples will show superparamagnetic behavior. Interestingly, for these superparamagnetic $La_{0.6}Pb_{0.4}MnO_3$ nanoparticles, they show memory effects in the *dc* magnetization and magnetic relaxation.[144]

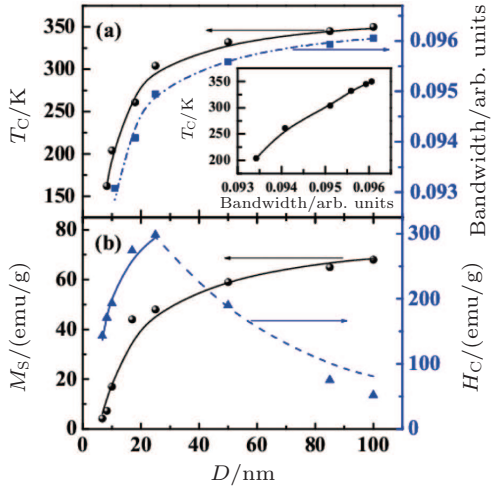



**Fig. 28.** (a) Particle-size dependencies of ferromagnetic transition temperature $T_C$ and bandwidth $W_{O_{2p}}$ for $La_{0.6}Pb_{0.4}MnO_3$ nanoparticles. The solid line is the calculated result using Eq. (6) and the dash–dot line is obtained by Eq. (7). Inset of (a) shows $W_{O_{2p}}$ dependence of $T_C$; the line is a guide for the eyes. (b) Variations of $M_S$ and $H_C$ as a function of particle size.[141]

### 4.2. Nanosized-induced CO melting and exchange bias effect in $La_{0.25}Ca_{0.75}MnO_3$ nanoparticles

For charge ordered manganites, it is believed that the stability of CO state is strong with the collinear AFM ordering of the localized Mn moments.[145] When the size is reduced to nanoscale, the uncompensated surface spins will destroy the long range collinear AFM configuration,[146] which, in turn, would impede the CO state. A series of experiments have confirmed that with decreasing particle size there is a suppression of the CO states accompanied with a reduction of AFM phase as well as the appearance of FM phase in nanosized $La_{0.4}Ca_{0.6}MnO_3$,[147] $Nd_{0.5}Ca_{0.5}MnO_3$,[148] and $Pr_{0.5}Ca_{0.5}MnO_3$ systems,[149] etc.

It is known that the CO state in bulk $La_{0.25}Ca_{0.75}MnO_3$ compound is very stable; see Fig. 9.[61] However, for nanosized $La_{0.25}Ca_{0.75}MnO_3$, the CO transition gradually shifts to lower temperature with decreasing particle size ($D$); meanwhile, the ferromagnetic cluster glass state appears,[151] and the spin cluster glass temperature $T_G$ shows a nonmonotonous variation with $D$ as shown in Fig. 29.[150,152] The variations of $T_{CO}$ and $T_G$ with particle size can be explained by the improved core-shell model.[153] As illustrated in Fig. 30, bulk $La_{0.25}Ca_{0.75}MnO_3$ is of almost a perfect AFM spin ordering, while for an $La_{0.25}Ca_{0.75}MnO_3$ nanoparticle, a larger number of uncompensated surface spins appear, and the shell spins will deviate from the AFM arrangement of the core spins, which weakens the AFM interaction across the shell and hence enhances the FM interaction.[150] The enhanced FM coupling facilitates the formation of FM cluster glass in these regions, and thus the temperature $T_G$ for the appearance of ferromagnetic clusters increases with decreasing particle size. However, with particle size decreasing further, the surface spins become more disordered and thus disfavor the FM coupling, resulting in a decrease of $T_G$ with the decrease of $D$.[141,148] Thus, when the two competing factors reach a balance, $T_G$ attains a maximum. The destruction of AFM configuration, on the other hand, will cause a reduction of $T_{CO}$ with decreasing the particle size.[150] Furthermore, from the frequency and DC magnetic field dependencies of the AC susceptibilities of $La_{0.25}Ca_{0.75}MnO_3$ nanoparticles, one can find that the FM cluster size in the shell of the nanoparticles increases with decreasing particle size within a certain size range.[136]

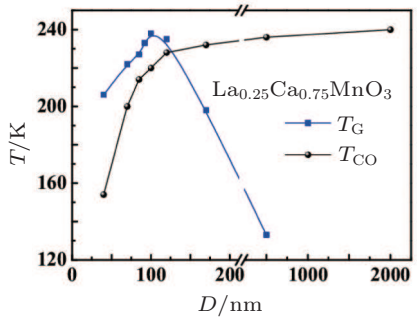



**Fig. 29.** Temperature versus particle size phase of $La_{0.25}Ca_{0.75}MnO_3$. The solid lines are guides for the eyes.[150]

Because of the coexistence of FM clusters and AFM phase, the exchange bias (EB) effect should be observed in those manganite nanoparticles.[154,155] Figure 31 shows the particle diameter $D$ dependencies of exchange bias field ($H_{EB}$) and coercivity ($H_C$) for $La_{0.25}Ca_{0.75}MnO_3$ at different temperatures.[154] It can be seen that with increasing temperature, $H_{EB}$ decreases and the peak height diminishes gradually but the peak position (around 80 nm) changes only inconspicuously. It is believed that the exchange coupling is closely related to the uncompensated interfacial spins, FM/AFM interfacial pinning strength and the AFM anisotropy energy. Thus, the diameter dependencies of $H_{EB}$ can be well explained in terms of the core-shell model in Fig. 30. However, the position of the $H_C$ peak shifts to a larger particle size with increasing temperature, unlike that of $H_{EB}$.

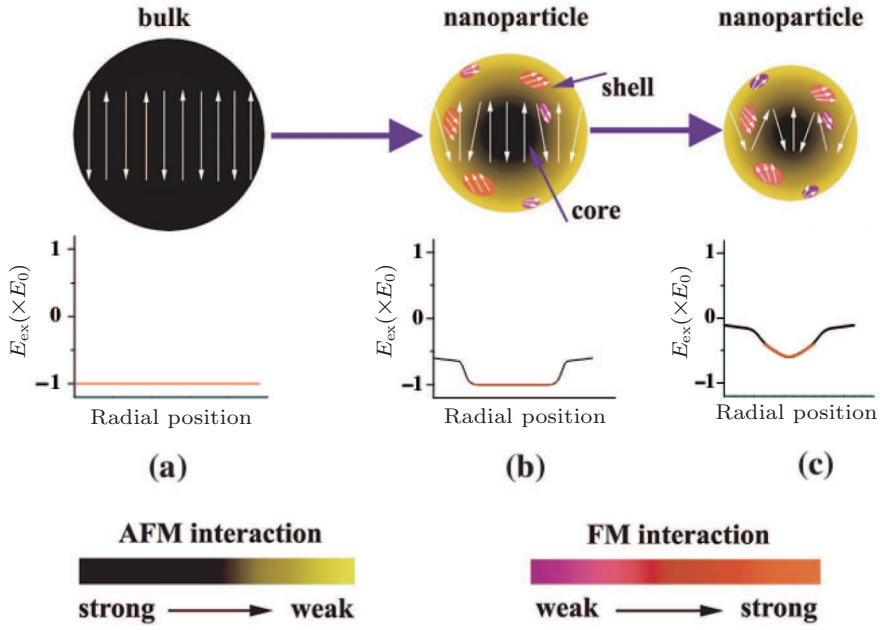



**Fig. 30.** Schematic diagrams (two-dimensional) for evolutions of the magnetic configuration, the exchange energy, and magnetic interactions with particle size, proposed on the basis of the core-shell model in Ref. [153]. Arrows represent only the spin orientations. (a) Perfect AFM spin ordering in bulk $La_{0.25}Ca_{0.75}MnO_3$, assuming the AFM exchange energy $E_{ex} = -E_0$. (b) For nanoparticles, the core spins are nearly antiparallel. The deviation of shell spins from the AFM arrangement makes the $E_{ex}$ value less negative and leads to the formation of FM clusters across the shell regions. (c) For smaller nanoparticles, more disordered shell spins not only induce the deviation of core spins from the AFM arrangement and accordingly further increase $E_{ex}$ value but also weaken the FM coupling greatly.[150]

From the results mentioned above, one can see that there are some basic topics with regard to manipulating physical properties that need further investigation, although the distinct physical and chemical properties of nanosized CMR manganites already show potential applicability in both mesoscopic physics and nanodevices.[156–158]

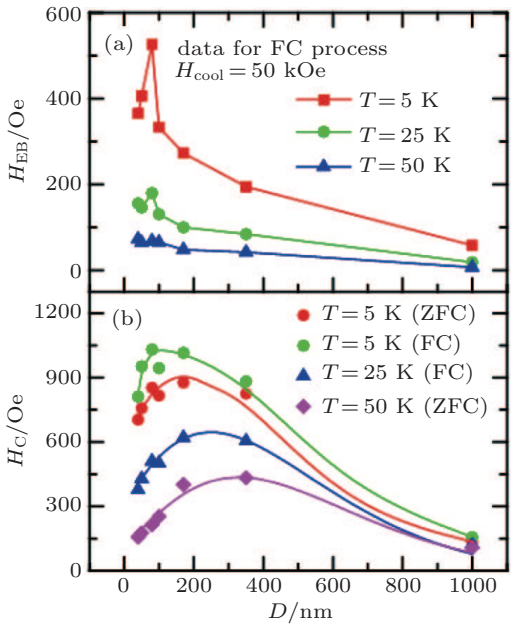



**Fig. 31.** Particle diameter dependencies of (a) exchange bias field $H_{EB}$ measured at 5, 25, and 50 K in FC processes for $La_{0.25}Ca_{0.75}MnO_3$, and (b) coercivity $H_C$ measured at 5 K in ZFC and FC processes and at 25 K and 50 K in FC processes. The solid lines are guides for the eyes.[154]

## 5. Conclusion and remarks

In summary, the colossal magnetoresistance effects in manganites that are related to the metal–insulator transition and the disarrangement of the charge ordered state in magnetic fields were discussed. We proposed a phenomenological model describing the relationship between phase separation and magnetoresistance, which shows that the competition between the metallic and insulating phases plays an important role in the CMR effect. Based on the CMR effect and high spin-polarization in manganites, some prototype devices have been fabricated and show potential applications in multifunctional spintronics. In the manganite/Nb:STO p–n junctions, an electric field- and temperature-tuned positive/negative magnetoresistance effect arising from the band structure change at the manganites-Nb:STO interface was discussed. Using ferromagnetic manganites as metallic electrodes in multiferroic heterostructures, one can realize ferroelectric and magnetic field controlled electric and magnetic properties of manganites as well as manganite/ferroelectric heterostructures. We described the potential for practical applications of the half-metallic property of manganites, the high TMR effect in magnetic tunnel junctions, the four nonvolatile states and magnetoelectric coupling in multiferroic tunnel junctions, and spin detectors in organic spin-valves. In addition, the effect of nanoparticle size on FM $La_{0.6}Pb_{0.4}MnO_3$ nanoparticles and magnetic properties in the CO $La_{0.25}Ca_{0.75}MnO_3$ system were discussed.

The CMR manganites show rich physics with complex electronic, magnetic, and structural phase diagrams and great potential for applications in multifunctional spintronics; however, from the industrial viewpoint, some obstacles have to be overcome: (i) Integrating the newly observed phenomena in CMR manganites, such as the magnetoelectric coupling, spin-dependent tunneling, resistance switching, spin transfer torque, etc., to realize low-field high magnetoresistance effect, new functionality and high memory density. (ii) Incorporating prototype devices that are based on colossal magnetoresistance onto a semiconductor chip without sacrificing the emergent phenomena in the manganites. (iii) Coping with the energy required for fabrication. Compared to bulk samples, high quality films show much more powerful application prospects, such as in tunnel junctions and spin-valves. However, the high growth temperature (usually 700 °C or higher) for preparing the high quality thin films by sputtering, molecular epitaxy, pulsed laser deposition, etc., requires high energy expenditures, and such temperatures are not currently used in conventional processes of microelectronics.

To resolve these issues, a considerable research has already been done. For example, low-temperature synthesis methods, such as the sol–gel technique,[159,160] chemical solution deposition,[161,162] wet-chemical methods,[163] etc., have been developed to fabricate CMR manganite films on single crystals. In order to integrate perovskite-type manganites onto silicon, different templates or buffer layers between the CMR layer and silicon, such as $Bi_4Ti_3O_{12}$,[164,165] $SrTiO_3$,[166–168] yttrium-stabilized zirconia (YSZ),[169,170] have been used. Despite all these studies, the problems remain problems from an industrial point of view, and further studies are needed for exploring new materials and new technologies.

## References


[1] Ramirez A P 1997 *J. Phys.: Condens. Matter* **9** 8171
[2] Imada M, Fujimori A and Tokura Y 1998 *Rev. Mod. Phys.* **70** 1039
[3] Coey J M D, Viret M and Molnar S V 1999 *Adv. Phys.* **48** 167
[4] WPrellier P L A B M 2001 *J. Phys.: Condens. Matter* **13** R915
[5] Salamon M B and Jaime M 2001 *Rev. Mod. Phys.* **73** 583
[6] Tokura Y and Tomioka Y 1999 *J. Magn. Magn. Mater.* **200** 1
[7] Dagotto E, Hotta T and Moreo A 2001 *Phys. Rep.* **344** 1
[8] Haghiri-Gosnet A M and Renard J P 2003 *J. Phys. D: Appl. Phys.* **36** R127
[9] Tokura Y 2006 *Rep. Prog. Phys.* **69** 797
[10] Searle C W and Wang S T 1969 *Can. J. Phys.* **47** 2023
[11] Jin S, Tiefel T H, McCormack M, Fastnacht R A, Ramesh R and Chen L H 1994 *Science* **264** 413
[12] Jonker G H and Vansanten J H 1950 *Physica* **16** 337
[13] Jahn H A and Teller E 1937 *Proc. R. Soc. Lond. A: Math. Phys. Sci.* **161** 220
[14] Zener C 1951 *Phys. Rev.* **82** 403
[15] Hwang H Y, Cheong S W, Ong N P and Batlogg B 1996 *Phys. Rev. Lett.* **77** 2041
[16] Zhou T F, Li G, Wang N Y, Wang B M, Li X G and Chen Y 2006 *Appl. Phys. Lett.* **88** 232508
[17] Soulen R J Jr, Byers J M and Osofsky M S 1998 *Science* **282** 85
[18] Pissas M and Papavassiliou G 2004 *J. Phys.: Condens. Matter* **16** 6527
[19] Pissas M, Margiolaki I, Papavassiliou G, Stamopoulos D and Argyriou D 2005 *Phys. Rev. B* **72** 064425
[20] Mutou T and Kontani H 1999 *Phys. Rev. Lett.* **83** 3685
[21] Hotta T, Malvezzi A L and Dagotto E 2000 *Phys. Rev. B* **62** 9432
[22] Yunoki S, Hotta T and Dagotto E 2000 *Phys. Rev. Lett.* **84** 3714
[23] Schiffer P, Ramirez A P, Bao W and Cheong S W 1995 *Phys. Rev. Lett.* **75** 3336
[24] Chen C H and Cheong S W 1996 *Phys. Rev. Lett.* **76** 4042
[25] Mori S, Chen C H and Cheong S W 1998 *Nature* **392** 473
[26] Fath M, Freisem S, Menovsky A A, Tomioka Y, Aarts J and Mydosh J A 1999 *Science* **285** 1540
[27] Uehara M, Mori S, Chen C H and Cheong S W 1999 *Nature* **399** 560
[28] Papavassiliou G, Fardis M, Belesi M, Maris T G, Kallias G, Pissas M and Niarchos D 2000 *Phys. Rev. Lett.* **84** 761
[29] Kapusta C, Riedi P C, Sikora M and Ibarra M R 2000 *Phys. Rev. Lett.* **84** 4216
[30] Martin L W and Ramesh R 2012 *Acta Mater.* **60** 2449
[31] Vaz C A, Hoffman J, Ahn C H and Ramesh R 2010 *Adv. Mater.* **22** 2900
[32] Lu Y, Li X W, Gong G Q, Xiao G, Gupta A, Lecoeur P, Sun J Z, Wang Y Y and Dravid V P 1996 *Phys. Rev. B* **54** R8357
[33] Xiong Z H, Wu D, Vardeny Z V and Shi J 2004 *Nature* **427** 821
[34] McCormack M, Jin S, Tiefel T H, Fleming R M, Phillips J M and Ramesh R 1994 *Appl. Phys. Lett.* **64** 3045
[35] Jin S, Obryan H M, Tiefel T H, McCormack M and Rhodes W W 1995 *Appl. Phys. Lett.* **66** 382
[36] DeTeresa J M, Ibarra M R, Algarabel P A, Ritter C, Marquina C, Blasco J, Garcia J, delMoral A and Arnold Z 1997 *Nature* **386** 256
[37] Zuo J M and Tao J 2001 *Phys. Rev. B* **63** 060407
[38] La Spina A, Paolicchi P, Kryszczynska A and Pravec P 2004 *Nature* **428** 400
[39] Milward G C, Calderon M J C and Littlewood P B 2005 *Nature* **433** 607
[40] Sen C, Alvarez G and Dagotto E 2007 *Phys. Rev. Lett.* **98** 127202
[41] Allodi G, Renzi R D, Solzi M, Kamenev K, Balakrishnan G and Pieper M W 2000 *Phys. Rev. B* **61** 5924
[42] Radaelli P G, Ibberson R M, Argyriou D N, Casalta H, Andersen K H, Cheong S W and Mitchell J F 2001 *Phys. Rev. B* **63** 172419
[43] Lu Y, Li Q A, Di N L, Li R W, Ma X, Kou Z Q and Cheng Z H 2003 *Chin. Phys.* **12** 1301
[44] Li R W, Zhang Z R, Li Q A, Sun J R, Wang G J, Cheng Z H, Wang Z H, Zhang S Y, Han B S and Shen B G 2002 *J. Appl. Phys.* **92** 7404
[45] Patil S I, Bhagat S M, Shu Q Q, Lofland S E, Ogale S B, Smolyaninova V N, Zhang X, Palmer B S, Decca R S, Brown F A, Drew H D, Greene R L, Troyanchuk I O and McCarroll W H 2000 *Phys. Rev. B* **62** 9548
[46] Li G, Zhou H D, Feng S J, Fan X J, Li X G and Wang Z D 2002 *J. Appl. Phys.* **92** 1406
[47] Yuan S L, Li Z Y, Zhao W Y, Li G, Jiang Y, Zeng X Y, Yang Y P, Zhang G Q, Tu F, Tang C Q and Jin S Z 2001 *Phys. Rev. B* **63** 172415
[48] Jaime M, Lin A, Salamon M B and Han P D 1998 *Phys. Rev. B* **58** R5901
[49] Zhao G M, Smolyaninova V, Prellier W and Keller H 2000 *Phys. Rev. Lett.* **84** 6086
[50] Jia Y X, Lu L, Khazeni K, Crespi V H, Zettl A and Cohen M L 1995 *Phys. Rev. B* **52** 9147
[51] Liu Y K, Yao Y P, Dong S N, Yang S W and Li X G 2012 *Phys. Rev. B* **86** 075113
[52] Ward T Z, Liang S, Fuchigami K, Yin L F, Dagotto E, Plummer E W and Shen J 2008 *Phys. Rev. Lett.* **100** 247204
[53] Ward T Z, Zhang X G, Yin L F, Zhang X Q, Liu M, Snijders P C, Jesse S, Plummer E W, Cheng Z, Dagotto E and Shen J 2009 *Phys. Rev. Lett.* **102** 087201
[54] Ward T Z, Gai Z, Guo H W, Yin L F and Shen J 2011 *Phys. Rev. B* **83** 125125
[55] Tokura Y, Kuwahara H, Moritomo Y, Tomioka Y and Asamitsu A 1996 *Phys. Rev. Lett.* **76** 3184
[56] Tomioka Y, Asamitsu A, Kuwahara H, Moritomo Y and Tokura Y 1996 *Phys. Rev. B* **53** R1689
[57] Prellier W, Simon C, Haghiri-Gosnet A M, Mercey B and Raveau B 2000 *Phys. Rev. B* **62** R16337
[58] Tomioka Y and Tokura Y 2002 *Phys. Rev. B* **66** 104416
[59] Tomioka Y, Okimoto Y, Jung J H, Kumai R and Tokura Y 2003 *Phys. Rev. B* **68** 094417
[60] Zheng R K, Li G, Yang Y, Tang A N, Wang W, Qian T and Li X G 2004 *Phys. Rev. B* **70** 014408

[61] Li X G, Zheng R K, Li G, Zhou H D and Huang R X 2002 *Europhys. Lett.* **60** 670
[62] Tomioka Y, Asamitsu A, Moritomo Y, Kuwahara H and Tokura Y 1995 *Phys. Rev. Lett.* **74** 5108
[63] Qian T, Zheng R K, Zhang T, Zhou T F, Wu W B and Li X G 2005 *Phys. Rev. B* **72** 024432
[64] Chen P and Du Y W 2001 *Chin. Phys.* **10** 970
[65] Huang X H, Jiang Z L, Sun X F and Li X G 2011 *J. Am. Ceram. Soc.* **94** 1324
[66] Nogues J and Schuller I K 1999 *J. Magn. Magn. Mater.* **192** 203
[67] Tanaka H, Zhang J and Kawai T 2002 *Phys. Rev. Lett.* **88** 027204
[68] Xie Y W, Guo D F, Sun J R and Shen B G 2010 *Chin. Phys. B* **19** 117306
[69] Mitra C, Raychaudhuri P, Dörr K, Müller K H, Schultz L, Oppeneer P and Wirth S 2003 *Phys. Rev. Lett.* **90** 017202
[70] Jin K J, Lu H B, Zhou Q L, Zhao K, Cheng B L, Chen Z H, Zhou Y L and Yang G Z 2005 *Phys. Rev. B* **71** 184428
[71] Sheng Z G, Song W H, Sun Y P, Sun J R and Shen B G 2005 *Appl. Phys. Lett.* **87** 032501
[72] Katsu H, Tanaka H and Kawai T 2000 *Appl. Phys. Lett.* **76** 3245
[73] Sun J R, Xiong C M, Zhao T Y, Zhang S Y, Chen Y F and Shen B G 2004 *Appl. Phys. Lett.* **84** 1528
[74] Lu H B, Yang G Z, Chen Z H, Dai S Y, Zhou Y L, Jin K J, Cheng B L, He M, Liu L F, Guo H Z, Fei Y Y, Xiang W F and Yan L 2004 *Appl. Phys. Lett.* **84** 5007
[75] Zhou T F, Li G, Qian T and Li X G 2006 *Appl. Phys. Lett.* **89** 222504
[76] Zhao K, Jin K J, Lu H B, He M, Huang Y H, Yang G Z and Zhang J D 2008 *Appl. Phys. Lett.* **93** 252110
[77] Mathews S, Ramesh R, Venkatesan T and Benedetto J 1997 *Science* **276** 238
[78] Liu Y K, Yao Y P, Dong S N, Jiang T, Yang S W and Li X G 2012 *Thin Solid Films* **520** 5775
[79] Wu T, Ogale S, Garrison J, Nagaraj B, Biswas A, Chen Z, Greene R, Ramesh R, Venkatesan T and Millis A 2001 *Phys. Rev. Lett.* **86** 5998
[80] Zheng R K, Wang Y, Chan H L W, Choy C L and Luo H S 2008 *Appl. Phys. Lett.* **92** 082908
[81] Thiele C, Dörr K, Fähler S, Schultz L, Meyer D C, Levin A A and Paufler P 2005 *Appl. Phys. Lett.* **87** 262502
[82] Thiele C, Dörr K, Schultz L, Beyreuther E and Lin W M 2005 *Appl. Phys. Lett.* **87** 162512
[83] Zheng R K, Wang Y, Wang J, Wong K S, Chan H L W, Choy C L and Luo H S 2006 *Phys. Rev. B* **74** 094427
[84] Eerenstein W, Wiora M, Prieto J L, Scott J F and Mathur N D 2007 *Nat. Mater.* **6** 348
[85] Thiele C, Dörr K, Bilani O, Rödel J and Schultz L 2007 *Phys. Rev. B* **75** 054408
[86] Zhu Q X, Wang W, Yang S W, Li X M, Wang Y, Habermeier H U, Luo H S, Chan H L W, Li X G and Zheng R K 2012 *Appl. Phys. Lett.* **101** 172906
[87] Zheng R K, Habermeier H U, Chan H L W, Choy C L and Luo H S 2010 *Phys. Rev. B* **81** 104427
[88] Yang Y J, Yang M M, Luo Z L, Huang H L, Wang H B, Bao J, Hu C S, Pan G Q, Yao Y P, Liu Y K, Li X G, Zhang S, Zhao Y G and Gao C 2012 *Appl. Phys. Lett.* **100** 043506
[89] Yang Y J, Luo Z L, Yang M M, Huang H L, Wang H B, Bao J, Pan G Q, Gao C, Hao Q, Wang S T, Jokubaitis M, Zhang W Z, Xiao G, Yao Y P, Liu Y K and Li X G 2013 *Appl. Phys. Lett.* **102** 033501
[90] Vaz C A F, Hoffman J, Segal Y, Reiner J W, Grober R D, Zhang Z, Ahn C H and Walker F J 2010 *Phys. Rev. Lett.* **104** 127202
[91] Molegraaf H J A, Hoffman J, Vaz C A F, Gariglio S, van der Marel D, Ahn C H and Triscone J M 2009 *Adv. Mater.* **21** 3470
[92] Yu P, Lee J S, Okamoto S, Rossell M, Huijben M, Yang C H, He Q, Zhang J, Yang S, Lee M, Ramasse Q, Erni R, Chu Y H, Arena D, Kao C C, Martin L and Ramesh R 2010 *Phys. Rev. Lett.* **105** 027201
[93] Wu S M, Cybart S A, Yu P, Rossell M D, Zhang J X, Ramesh R and Dynes R C 2010 *Nat. Mater.* **9** 756
[94] Eerenstein W, Mathur N D and Scott J F 2006 *Nature* **442** 759
[95] Kamba S, Nuzhnyy D, Savinov M, Šebek J, Petzelt J, Prokleška J, Haumont R and Kreisel J 2007 *Phys. Rev. B* **75** 024403
[96] Le Bras G, Colson D, Forget A, Genand-Riondet N, Tourbot R and Bonville P 2009 *Phys. Rev. B* **80** 134417
[97] Bowen M, Bibes M, Barthélémy A, Contour J P, Anane A, Lemaître Y and Fert A 2003 *Appl. Phys. Lett.* **82** 233
[98] Wu D, Xiong Z H, Li X G, Vardeny Z and Shi J 2005 *Phys. Rev. Lett.* **95** 016802
[99] Wang F J, Yang C G, Vardeny Z and Li X G 2007 *Phys. Rev. B* **75** 245324
[100] Obata T, Manako T, Shimakawa Y and Kubo Y 1999 *Appl. Phys. Lett.* **74** 290
[101] Teresa J M D, Barthélémy A, Fert A, Contour J P, Lyonnet R, Montaigne F, Seneor P and Vaur'es A 1999 *Phys. Rev. Lett.* **82** 4288
[102] De Teresa J M, Barthélémy A, Fert A, Contour J P, Montaigne F and Seneor P 1999 *Science* **286** 507
[103] Sefrioui Z, Visani C, Calderon M J, March K, Carretero C, Walls M, Rivera-Calzada A, Leon C, Anton R L, Charlton T R, Cuellar F A, Iborra E, Ott F, Imhoff D, Brey L, Bibes M, Santamaria J and Barthelemy A 2010 *Adv. Mater.* **22** 5029
[104] Zhuravlev M Y, Sabirianov R F, Jaswal S S and Tsymbal E Y 2005 *Phys. Rev. Lett.* **94** 246802
[105] Kohlstedt H, Pertsev N A, Contreras J R and Waser R 2005 *Phys. Rev. B* **72** 125341
[106] Tsymbal E Y and Kohlstedt H 2006 *Science* **313** 181
[107] Garcia V, Fusil S, Bouzehouane K, Enouz-Vedrenne S, Mathur N D, Barthelemy A and Bibes M 2009 *Nature* **460** 81
[108] Maksymovych P, Jesse S, Yu P, Ramesh R, Baddorf A P and Kalinin S V 2009 *Science* **324** 1421
[109] Chanthbouala A, Crassous A, Garcia V, Bouzehouane K, Fusil S, Moya X, Allibe J, Dlubak B, Grollier J, Xavier S, Deranlot C, Moshar A, Proksch R, Mathur N D, Bibes M and Barthelemy A 2012 *Nat. Nanotechnol.* **7** 101
[110] Velev J P, Duan C G, Burton J D, Smogunov A, Niranjan M K, Tosatti E, Jaswal S S and Tsymbal E Y 2009 *Nano Lett.* **9** 427
[111] Tsymbal E Y, Gruverman A, Garcia V, Bibes M and Barthelemy A 2012 *MRS Bull.* **37** 138
[112] Garcia V, Bibes M, Bocher L, Valencia S, Kronast F, Crassous A, Moya X, Enouz-Vedrenne S, Gloter A, Imhoff D, Deranlot C, Mathur N D, Fusil S, Bouzehouane K and Barthelemy A 2010 *Science* **327** 1106
[113] Valencia S, Crassous A, Bocher L, Garcia V, Moya X, Cherifi R O, Deranlot C, Bouzehouane K, Fusil S, Zobelli A, Gloter A, Mathur N D, Gaupp A, Abrudan R, Radu F, Barthelemy A and Bibes M 2011 *Nat. Mater.* **10** 753
[114] Hambe M, Petraru A, Pertsev N A, Munroe P, Nagarajan V and Kohlstedt H 2010 *Adv. Funct. Mater.* **20** 2436
[115] Pantel D, Goetze S, Hesse D and Alexe M 2012 *Nat. Mater.* **11** 289
[116] Yin Y W, Raju M, Hu W J, Weng X J, Zou K, Zhu J, Li X G, Zhang Z D and Li Q 2012 *Front. Phys.* **7** 380
[117] Yin Y W, Raju M, Hu W J, Weng X J, Li X G and Li Q 2011 *J. Appl. Phys.* **109** 07
[118] Yin Y W, Yao Y P and Li X G 2012 *Sci. China: Phys. Mech. Astron.* **42** 1185
[119] Duan C G, Jaswal S S and Tsymbal E Y 2006 *Phys. Rev. Lett.* **97** 047201
[120] Niranjan M K, Burton J D, Velev J P, Jaswal S S and Tsymbal E Y 2009 *Appl. Phys. Lett.* **95** 052501
[121] Kanki T, Tanaka H and Kawai T 2006 *Appl. Phys. Lett.* **89** 242506
[122] Yin Y W, Burton J D, Kim Y M, Borisevich A Y, Pennycook S J, Yang S M, Noh T W, Gruverman A, Li X G, Tsymbal E Y and Li Q 2013 *Nat. Mater.* **12** 397
[123] Burton J D and Tsymbal E Y 2011 *Phys. Rev. Lett.* **106** 157203
[124] Burton J D and Tsymbal E Y 2009 *Phys. Rev. B* **80** 174406
[125] Contreras J R, Kohlstedt H, Poppe U, Waser R, Buchal C and Pertsev N A 2003 *Appl. Phys. Lett.* **83** 4595
[126] Pramanik S, Stefanita C G, Patibandla S, Bandyopadhyay S, Garre K, Harth N and Cahay M 2007 *Nat. Nanotechnol.* **2** 216
[127] Bobbert P, Wagemans W, van Oost F, Koopmans B and Wohlgenannt M 2009 *Phys. Rev. Lett.* **102** 156604
[128] Nguyen T D, Hukic-Markosian G, Wang F, Wojcik L, Li X G, Ehrenfreund E and Vardeny Z 2010 *Nat. Mater.* **9** 345
[129] Nguyen T D, Basel T P, Pu Y J, Li X G, Ehrenfreund E and Vardeny Z V 2012 *Phys. Rev. B* **85** 245437
[130] Rolfe N J, Heeney M, Wyatt P B, Drew A J, Kreouzis T and Gillin W P 2009 *Phys. Rev. B* **80** 241201
[131] Nguyen T D, Wang F J, Li X G, Ehrenfreund E and Vardeny Z V 2013 *Phys. Rev. B* **87** 075205

[132] Balcells L, Fontcuberta J, Martínez B and Obradors X 1998 *Phys. Rev. B* **58** 14697

[133] Wang Y and Fan H J 2012 *Small* **8** 1060

[134] Katiyar P, Kumar D, Nath T K, Kvit A V, Narayan J, Chattopadhyay S, Gilmore W M, Coleman S, Lee C B, Sankar J and Singh R K 2001 *Appl. Phys. Lett.* **79** 1327

[135] Zhu T, Shen B G, Sun J R, Zhao H W and Zhan W S 2001 *Appl. Phys. Lett.* **78** 3863

[136] Huang X H, Ding J F, Jiang Z L, Yin Y W, Yu Q X and Li X G 2009 *J. Appl. Phys.* **106** 083904

[137] Mahesh R, Mahendiran R, Raychaudhuri A K and Rao C N R 1996 *Appl. Phys. Lett.* **68** 2291

[138] Zheng L, Li K B and Zhang Y H 1998 *Phys. Rev. B* **58** 8613

[139] Dutta A, Gayathri N and Ranganathan R 2003 *Phys. Rev. B* **68** 054432

[140] Shankar K S, Kar S, Subbanna G N and Raychaudhuri A K 2004 *Solid State Commun.* **129** 479

[141] Zhang T, Li G, Qian T, Qu J F, Xiang X Q and Li X G 2006 *J. Appl. Phys.* **100** 094324

[142] Medarde M, Mesot J, Lacorre P, Rosenkranz S, Fischer P and Gobrecht K 1995 *Phys. Rev. B* **52** 9248

[143] Kneller E F and Luborsky F E 1963 *J. Appl. Phys.* **34** 656

[144] Zhang T, Li X G, Wang X P, Fang Q F and Dressel M 2010 *Eur. Phys. J. B* **74** 309

[145] Tokunaga M, Miura N, Tomioka Y and Tokura Y 1998 *Phys. Rev. B* **57** 5259

[146] Kodama R H, Makhlouf S A and Berkowitz A E 1997 *Phys. Rev. Lett.* **79** 1393

[147] Lu C L, Dong S, Wang K F, Gao F, Li P L, Lü L Y and Liu J M 2007 *Appl. Phys. Lett.* **91** 032502

[148] Rao S S, Tripathi S, Pandey D and Bhat S V 2006 *Phys. Rev. B* **74** 144416

[149] Rao S S, Anuradha K N, Sarangi S and Bhat S V 2005 *Appl. Phys. Lett.* **87** 182503

[150] Zhang T, Zhou T F, Qian T and Li X G 2007 *Phys. Rev. B* **76** 174415

[151] Li X G, Fan X J, Ji G, Wu W B, Wong K H, Choy C L and Ku H C 1999 *J. Appl. Phys.* **85** 1663

[152] Li X G and Zhang T 2009 *Ceram. Int.* **35** 151

[153] Bhowmik R, Nagarajan R and Ranganathan R 2004 *Phys. Rev. B* **69** 054430

[154] Huang X H, Ding J F, Zhang G Q, Hou Y, Yao Y P and Li X G 2008 *Phys. Rev. B* **78** 224408

[155] Markovich V, Fita I, Wisniewski A, Puzniak R, Mogilyansky D, Titelman L, Vradman L, Herskowitz M and Gorodetsky G 2008 *Phys. Rev. B* **77** 054410

[156] Jugdersuren B, Kang S, DiPietro R S, Heiman D, McKeown D, Pegg I L and Philip J 2011 *J. Appl. Phys.* **109** 016109

[157] Li C, Lei B, Luo Z C, Han S, Liu Z Q, Zhang D H and Zhou C W 2005 *Adv. Mater.* **17** 1548

[158] Han S, Li C, Liu Z Q, Lei B, Zhang D H, Jin W, Liu X L, Tang T and Zhou C W 2004 *Nano Lett.* **4** 1241

[159] Bae S Y and Wang S X 1996 *Appl. Phys. Lett.* **69** 121

[160] Malavasi L, Mozzati M C, Polizzi S, Azzoni C B and Flor G 2003 *Chem. Mater.* **15** 5036

[161] Angappane S, Murugaraj P, Sethupathi K, Rangarajan G, Sastry V S, Chakkaravarthi A A and Ramasamy P 2001 *J. Appl. Phys.* **89** 6979

[162] Zhu X, Sun Y, Dai J and Song W 2006 *J. Phys. D: Appl. Phys.* **39** 2654

[163] Mishra A, Dutta A, Samaddar S and Gupta A K 2013 *Thin Solid Films* **534** 67

[164] Gu J Y, Kwon C, Robson M C, Trajanovic Z, Ghosh K, Sharma R P, Shreekala R, Rajeswari M, Venkatesan T, Ramesh R and Noh T W 1997 *Appl. Phys. Lett.* **70** 1763

[165] Kim J H, Khartsev S I and Grishin A M 2003 *Appl. Phys. Lett.* **82** 4295

[166] Pradhan A K, Mohanty S, Zhang K, Dadson J B, Jackson E M, Hunter D, Rakhimov R R, Loutts G B, Zhang J and Sellmyer D J 2005 *Appl. Phys. Lett.* **86** 012503

[167] Wong K H and Leung Y S 1999 *Thin Solid Films* **354** 55

[168] Belmeguenai M, Mercone S, Adamo C, Méchin L, Fur C, Monod P, Moch P and Schlom D G 2010 *Phys. Rev. B* **81** 054410

[169] Lang P L, Zhao Y G, Yang B, Zhang X L, Li J, Wang P and Zheng D N 2005 *Appl. Phys. Lett.* **87** 053502

[170] Kung P J, Fenner D B, Potrepka D M and Budnick J I 1996 *Appl. Phys. Lett.* **69** 427